THE SOCKET LENGTH OF PILES IN SOFT ROCK: A CASE STUDY

by

Hamdi Yılmaz

B.S., in C.E., Istanbul Technical University, 2004

Submitted to the Institute for Graduate Studies in
Science and Engineering in partial fulfillment of
the requirements for the degree of
Master of Science

Graduate Program in Civil Engineering

Boğaziçi University

2007

THE SOCKET LENGTH OF PILES IN SOFT ROCK:
A CASE STUDY

APPROVED BY:

Prof. H. Turan Durgunoğlu (Thesis Supervisor)	.....
Prof. Gülay Altay	.....
Prof. Günay Kocasoy	.....

DATE OF APPROVAL: 14.09.2007

ACKNOWLEDGEMENTS

I would like to express my sincere gratitude to my thesis supervisor, Prof. Dr. Turan Durgunoğlu. He has made this work possible in many ways by offering excellent guidance and support during this work. Without his understanding and friendly attitude, this study would not have been easy to handle.

I would also like to thank the members of my thesis committee, Prof. Dr. Gülay Altay and Prof. Dr. Günay Kocasoy, for their invaluable comments and suggestions.

I am also grateful to Zetaş Zemin Teknolojisi A.Ş., for providing the test site, equipment and great literature. The economic support provided by Zetaş Zemin Teknolojisi A.Ş. is greatly acknowledged.

I owe heartfelt gratitude to Selim İkiz, A. Cevdet Bayman, Özkan Kasımoğulları, Turhan Karadayılar, Barış Arkun and Canan Emrem Kulaç for their unchanging friendship, guidance and kind help during the last few years. Their sincere support has always encouraged and motivated me.

I am indebted to my officemates, Onur Ekli, Şahin Atmaca, Görkem İçöz, Önder Akçakal, Kayhan Aykın, Gülçin Özmen, Emel Hacıalioğlu, Gülden Yüksel, Figen Orhun, Şevket Tortop, Turgut Kaya and Saim Dudularoğlu for their generous help and friendship during the last two years. Without them, my life in last two years would have never been the same.

Finally, I would like to thank my family for their great patience, support and love during this study.

ABSTRACT

THE SOCKET LENGTH OF PILES IN SOFT ROCK: A CASE STUDY

In case where weak soil take place under mat foundations of high, heavily loaded structures, foundation system is designed with socket piles which transfer their load through skin friction to a firm stratum located at a considerable depth below the base of the structure. End bearing is generally not allowed for foundation piles of high structures for limiting vertical displacement conditions. Therefore the load of the structure is designed to be carried by friction between the firm stratum and the pile shaft. In literature there are different empirical relations for calculating unit friction resistance along the firm stratum.

In important applications, it is very crucial to obtain unit friction resistance values, their change with respect to depth by measurements, utilizing special pile load tests and prove that piles carry the load with a desired factor of safety within tolerable displacements. In this thesis, a case study is presented at Maslak, Istanbul which is named as the Mashattan project where ten 34 storey high rise residential blocks are planned to be constructed. The subsoil conditions consist of completely weathered, over consolidated clays(Belgrade Formation) which are located above the extensively fractured “graywacke” claystone- siltstone- sandstone formation, locally known as Trace Formation. Thickness of the Belgrade formations vary at the site, that is why friction between the soil and the pile shaft, with respect to depth and formation, needs to be determined. For that reason two special loading tests were performed just outside the foundation area and the test piles were loaded up to 6000 kN, which is twice the design load. In those tests, unit skin friction values are measured by taking strain measurements from the strain gauges which are installed at three different locations on the test piles. As a result, change of skin friction values with respect to depth is determined. Furthermore distribution of the applied load to skin and the tip are examined. By comparing calculated and measured unit skin friction values, safety of the design is tested prior to construction. Consequently, proper socket length of the pile to be utilized is determined.

ÖZET

YUMUŞAK KAYALARDA KAZIKLARIN SOKETLENME BOYU – BİR VAKA ANALİZİ

Yüksek yapılarda radye temeller altında belirli bir kalınlıkta nisbeten zayıf zemin yeralması halinde temel sistemi, taşıyıcı zemine belirli bir boyda soketlenen kazıklarla teşkil edilmektedir. Bu kazıkların, uç direncine genellikle kritik deplasman şartları nedeni ile müsade edilmediğinden, üst yapıdan gelen yüklerin münhasıran çeper sürtünmesi ile taşınması öngörülmektedir. Ancak literatürde geçmiş uygulamalarda kazıklar boyunca oluşabilecek birim sürtünme dirençleri için farklı görüşler bildirilmiş olup, bu nedenle tasarımda kullanılacak çeper birim sürtünme direncinin, önemli uygulamalarda ölçülerek tahkik edilmesi, birim çeper direncinin kazık boyunca dağılımının belirlenerek düşey proje kazık yüklerinin belirli bir güvenlikle taşındığının ispatlanması büyük önem arz etmektedir. Bu anlamda vaka analizi olarak sunulan bu makalede İstanbul Maslak'da Mashattan projesi kapsamında yapımı planlanan 34 katlı on adet yüksek bloğun üç adedinin altında çatlaklı kumtaşı-kiltaşı Trakya formasyonu üzerinde tamamen ayrışmış aşırı konsolide kil-kum seviyeleri içeren Belgrad formasyonu yeralmaktadır. Belgrad formasyonunun ve ayrışmış grovakların kalınlığının da değişken olması nedeni ile, birim çeper sürtünmesinin her iki formasyonda kazık boyunca dağılımının belirlenmesi gerekmiştir. Bu maksatla, blok dışında, tasarımı tahkik amaçlı özel iki adet kazık yükleme deneyi yapılmış, kazıklar tasarım yüklerinin iki katı olan 6000 kN'a kadar yüklenmiştir. Bu deneylerde, birim çeper sürtünme dirençleri deney kazığı boyunca , donatı üzerine özel bir şekilde yerleştirilen, birim deformasyon ölçer-strain gauge'ler vasıtasıyla, deformasyonlarını izlemek suretiyle ölçülmüştür. Sonuçta, çeper direncinin derinlikle dağılımı bulunmuş ve tatbik edilen yükün, ne kadarının kazık çeperi ve ucu arasında paylaşıldığı belirlenmiştir. Ölçülen değerler tasarımda kullanılan birim çeper direnci değerleri ile mukayese edilerek tasarımın güvenliliği uygulama öncesi tahkik edilmiştir.

TABLE OF CONTENTS

LIST OF FIGURES

LIST OF TABLES

LIST OF SYMBOLS/ABBREVIATIONS

c	Cohesion
C_B	Correction factor for bore diameter
C_E	Correction to account for rod energy
C_N	Correction factor for effective overburden stress
C_R	Correction factor for rod length
C_S	Correction Factor for the sampling method
c_u	Undrained Shear Strength
D	Depth factor
E_c	Concrete Young's modulus
E_m	Elastic modulus of rock mass
E_r	Elastic modulus of intact rock mass
f	Frequency
g	Aperture of the discontinuities
G	Gauge factor
h_m	Average roughness height of the shaft
i_m	Average asperity angle
i_{sd}	Standard deviation of asperity angles
j	Correction factor depending on normalized spacing of discontinuities
K_b	Empirical non-dimensional coefficient
K_{sp}	Empirical factor
L	Nominal length
L_t	Total travel length along the shaft wall profile
m_b	Strength parameter for the Hoek-Brown strength criterion
n	Modulus ratio
N	Measured standard penetration test blow count
p_0	At rest horizontal stress in the rock at the elevation of the shaft base

p_a	Atmospheric pressure
p_1	Limit pressure as determined from pressuremeter test
q_{max}	End bearing capacity
Q_u	Ultimate axial load of a drilled shaft related to rock
Q_{ub}	Ultimate end bearing load of a drilled shaft related to rock
Q_{us}	Ultimate shear load of a drilled shaft related to rock
s	Strength parameter for the Hoek-Brown Strength Criterion
S	Sensitivity Factor
α_c	Adhesion factor
α_w	Reduction factor reflecting the strength of the rock
α	Empirical factor for side shear resistance
α_w	Reduction factor reflecting the strength of the rock
β	Empirical factor for side shear resistance
β_w	Ratio of side shear resistance of jointed rock mass
η_c	Construction method reduction factor
ν	Poisson's ratio
ϕ	Internal Friction Angle
ψ	Coefficient of determination
ρ	Material density
σ_0	Total overburden stress at elevation of the shaft base
σ_c	Unconfined compressive strength of rock
σ_n	Initial normal stress on the shaft-rock interface
τ_{max}	Side shear resistances of drilled shafts
ER	Actual energy ratio
RF	Roughness Factor
RQD	Rock quality designation
SRC	Shaft resistance coefficient

1. INTRODUCTION

Drilled shafts is a foundation technique to transfer the structural loads to underlying rock mass. Especially when the foundation level soil is overburden and is not capable to carry the foundation loads. In addition to limit vertical displacements of heavy loaded structures drilled piles is chosen as a deep foundation technique. In the design phase of foundation piles, both load capacity and vertical displacement behavior under loading should be considered.

Axially loaded drilled shafts in rock are designed to transfer loads to rock mass by side shear, by end bearing or by combination of end bearing and side shear. To obtain end bearing, relatively large pile settlement is needed but the full side shear is obtained at much lower displacements. In other words, the settlement needed to obtain side shear is relatively very small compared to the settlement needed to obtain end bearing. High rise buildings are both heavy and sensitive to vertical displacement at foundation level. That is why the foundation piles for such structures are designed to carry safe working load by side shear only.

In this study design of piles in soft rock is reviewed and behavior of piles in soft rock is discussed and a case study is presented. The planned structures and structural properties together with subsoil modeling are summarized in chapter two. In chapter three, the pile design computational methods are summarized and pile design criteria is discussed for the case study. As case study a special pile testing procedure for vertical pile load capacity is identified in chapter four. Safe working load, design verification load, equipment for pile testing and test methodology are summarized. In the fifth and sixth chapters, case study evaluations for Mashattan Blocks A4, and A5 are discussed respectively. The final chapter summarizes the conclusions of this study.

2. PLANNED STRUCTURES

2.1. Introduction

In Maslak district of Istanbul, within Mashattan project, ten residential blocks with varying foundation levels are planned to be constructed on a site covering an area of approximately 140.000 square meters. Site location aerial view is shown on Figure 2.1.

The topographical elevations at the site vary from +58.00m to +102.0m; therefore, the approximate elevation difference between the lowest and highest points of the site is in the order of 44.0m.

Figure 2.1. Site Location aerial view for Mashattan Project

The subject development compromises ten residential blocks (A1 to A5, B1 to B5) which are planned to be constructed. The blocks were planned to be constructed with three to five basements, which will provide shelter, parking and space for electro-mechanical units. The blocks consist of ground floor and 31 stories. Layout plan, virtual preview of

the blocks and typical architectural section of the blocks are given in figures 2.2 to 2.4 respectively.

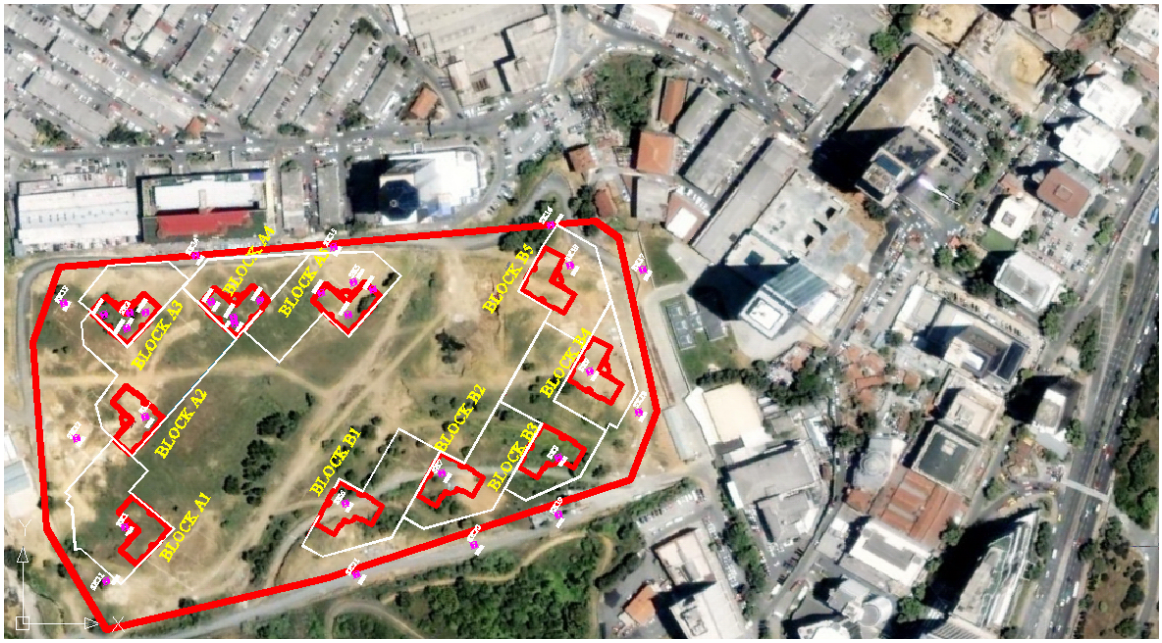

Figure 2.2. Layout plan for ten residential blocks in Mashattan Project

Figure 2.3. Virtual preview of the Mashattan blocks

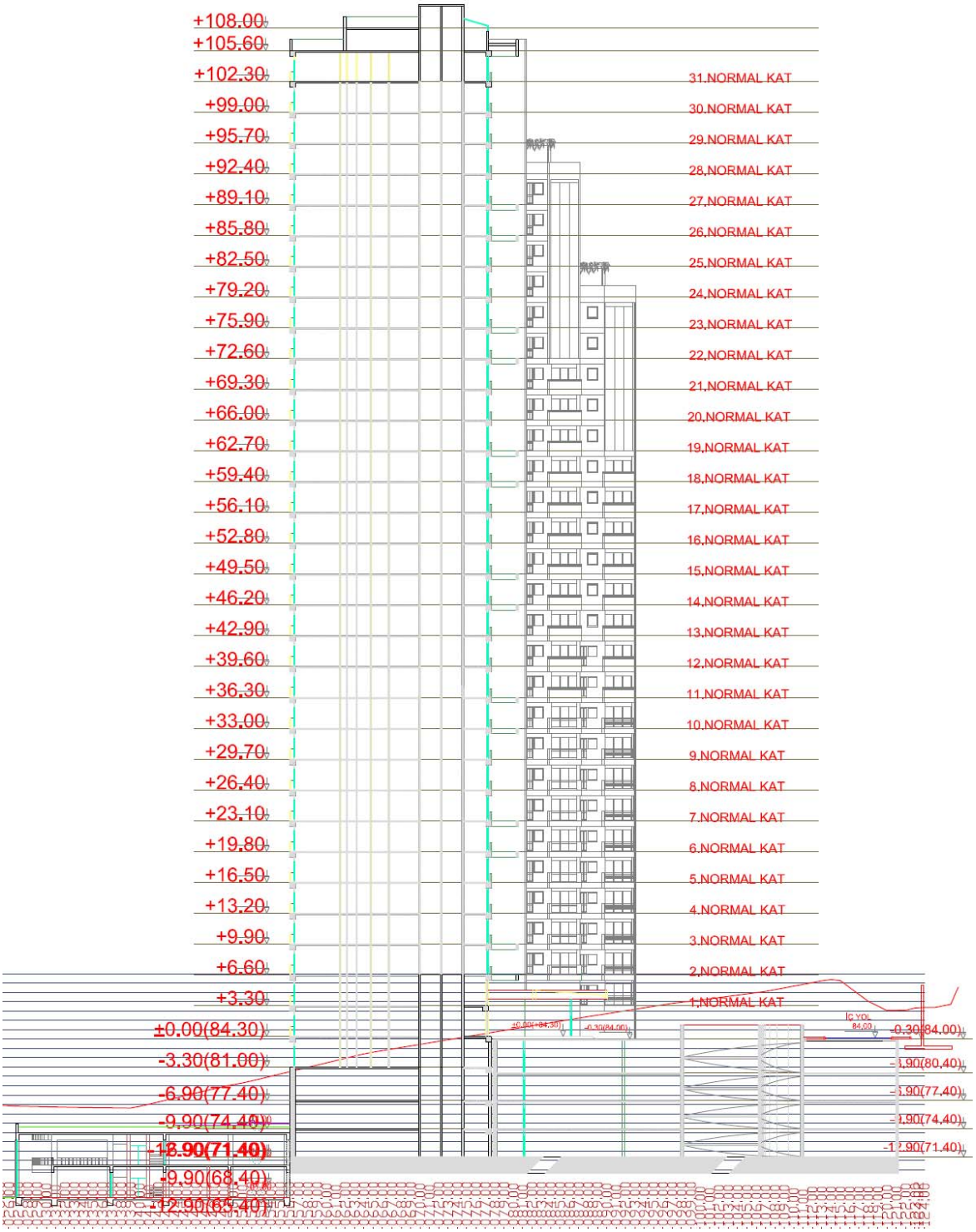

Figure 2.4. Typical architectural section of the blocks

Land elevations and lowest basement floor depths of the blocks together with the soil formations at the foundation levels are summarized in Table 2.1.

Table 2.1. Foundation information for ten blocks

Block ID	Lowest Basement Slab Upper Elevation (m)	Foundation Thickness (m)	Approximate Excavation Base Elevation	Minimum Site Elevation	Minimum Excavation Height (m)	Maximum Site Elevation	Maximum Excavaiton Height (m)	Formation at Foundation Level	Strength
A1	54.40	2.00	52.40	58.00	5.60	77.00	24.60	Trace Formation	medium
A2	65.40	2.00	63.40	77.00	13.60	85.00	21.60	Trace Formation	very weak
A3	68.40	2.00	66.40	80.00	13.60	88.00	21.60	Belgrad Formation (silt-sand N=40)	dense- compact
A4	71.40	2.00	69.40	80.00	10.60	90.00	20.60	Belgrad Formation (silt N>50)	dense- compact
A5	68.40	2.00	66.40	74.00	7.60	89.00	22.60	Trace	very weak - medium
B1	61.40	2.00	59.40	64.00	4.60	80.00	20.60	Trace	medium strength / weak-medium weak
B2	64.40	2.00	62.40	74.00	11.60	82.00	19.60	Trace	very weak - weak-medium
B3	70.40	2.00	68.40	77.00	8.60	91.00	22.60	Trace	very weak - medium
B4	76.40	2.00	74.40	83.00	8.60	95.00	20.60	Trace	very weak - weak
B5	70.40	2.00	68.40	81.00	12.60	93.00	24.60	Trace	very weak

2.2. Subsoil Modeling

Based on the size of the site, locations of the structures and different foundation elevations were taken into account, soil investigation was planned and executed in two phases. In the first phase, in addition to the general geotechnical modeling of the site, soil conditions nearby retaining structures were determined. Moreover, from the geotechnical modeling, the formations below the foundation elevations were evaluated. In the construction phase of the retaining structures i.e., during the second phase of soil investigations great amount of excavations were already performed, consequently three additional borings per block were drilled to complement the existing information about the soil conditions obtained during the first phase.

2.2.1. Subsoil Investigations

For soil investigations, at the initial first phase 21 borings having total length of 519m were performed.

Foundations of the blocks A1, A2, B1, B2, B3, B4 and B5 were recommended to be constructed as raft foundations considering that they are located on Trace Formation composed of fractured, mudstone, siltstone, sandstone greywacke formation.

Subsoil investigation locations including the blocks A4 and A5, where the extensive pile testing programme were performed, are presented in Figure 2.5. On the other hand summary of second phase boreholes including borehole length, coordinate and elevations for blocks A4 and A5 is given in Table 2.2. Detailed borehole logs are given in Encl-2.

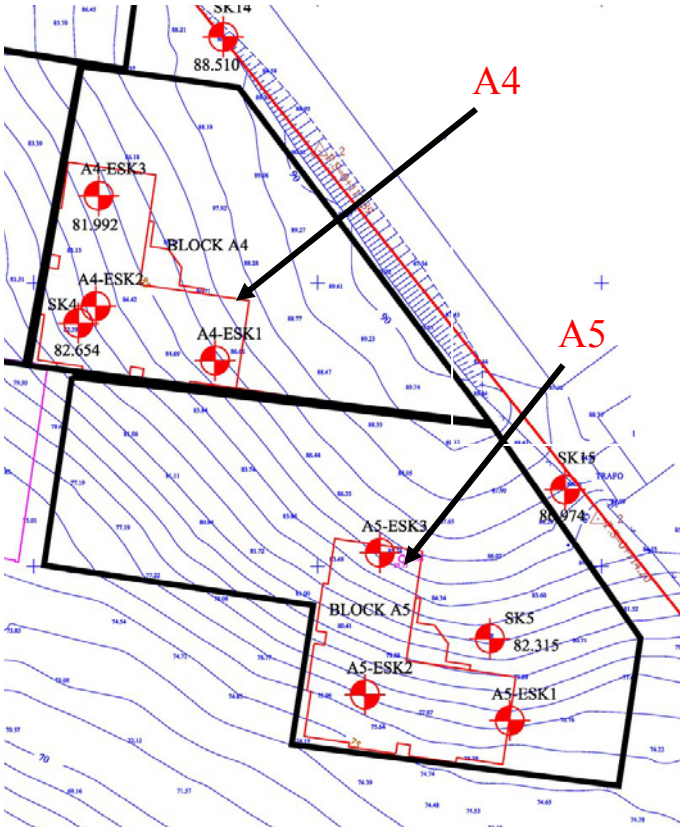

Figure 2.5. Subsoil investigation locations

Table 2.2. Summary of 2nd phase boreholes for Blocks A4 and A5.

Point ID	Hole Depth (m)	Elevation (m)	North	East	Date Started	Date Completed	Groundwater Depth (m)	Groundwater Elevation (m)
A-4 ESK-1	17.50	71.05	4553786.29	417431.94	20.10.2005	21.10.2005	1.60	69.45
A-4 ESK-2	17.50	71.32	4553795.89	417410.93	15.10.2005	16.10.2005	4.00	67.32
A-4 ESK-3	17.50	71.30	4553815.37	417411.44	18.10.2005	19.10.2005	2.15	69.15
A-5 ESK-1	13.60	70.40	4553722.77	417483.84	21.10.2005	22.10.2005	3.80	66.60
A-5 ESK-2	12.67	69.47	4553727.37	417458.34	13.10.2005	16.10.2005	3.10	66.37
A-5 ESK-3	12.28	69.08	4553752.39	417460.96	18.10.2005	21.10.2005	2.50	66.58
A4-SK-4	26.00	82.65	4553792.88	417407.87	09.03.2005	12.03.2005	7.20	75.45
A5-SK-5	22.00	82.32	4553737.27	417480.34	01.03.2005	04.03.2005	4.30	78.02

2.2.2. General Geology

The subject site is in Istanbul sheet of Turkey Geology Map with 1/500,000 scale. It is located in Istanbul peninsula. Geological units within Istanbul peninsula start with Early Paleozoic and continue conformably from Silurian through lower Carboniferous. This sequence is overlaid by the Triassic sedimentary rocks uncomfortably. Paleozoic aged units generally comprise detrital, carbonaceous rocks of Dolayoba, Kartal, Baltalimanı and Trace Formations. General geology map of the investigation site area is given in Figure2.6.

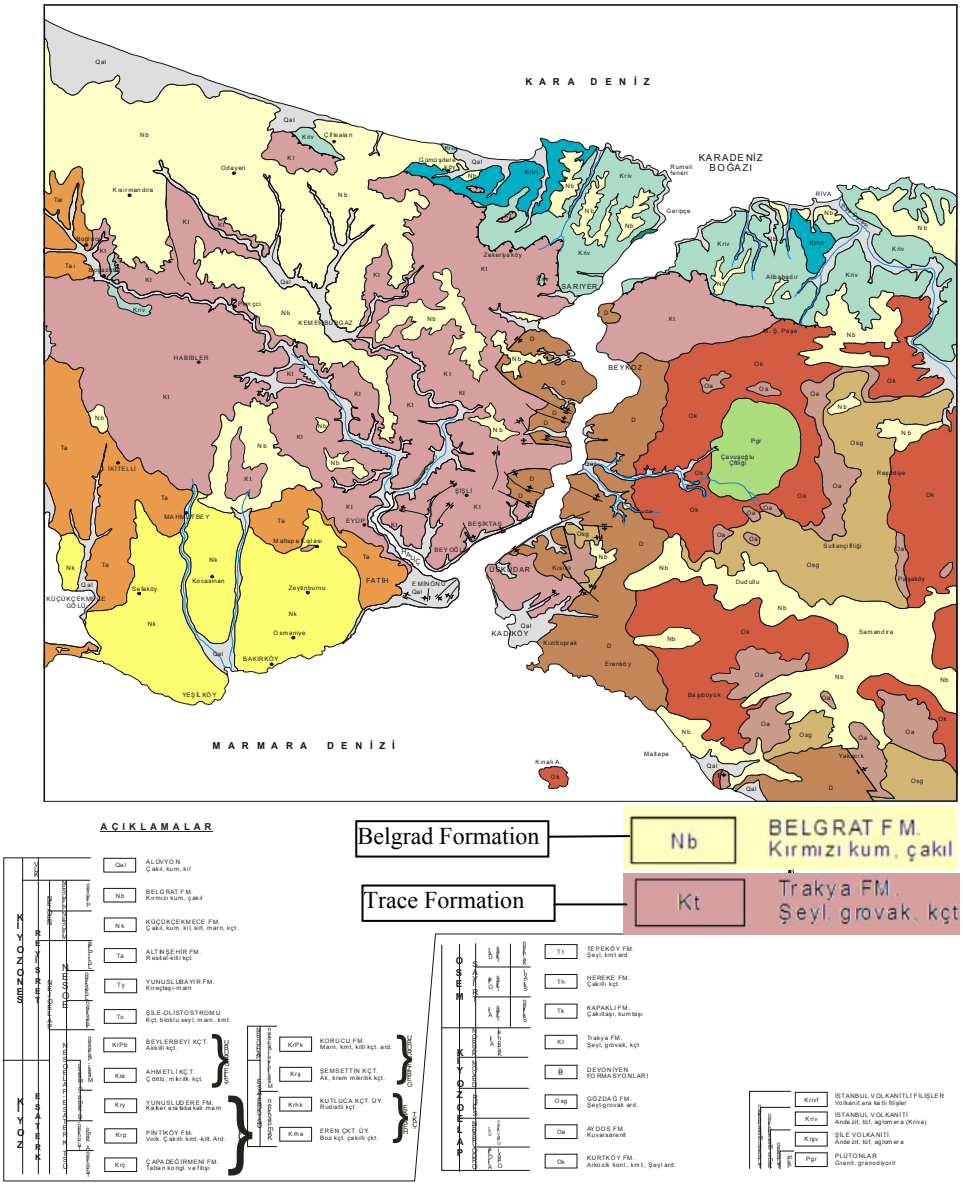

Figure 2.6. General geology map

The Dolayoba Formation aged Silurian is the oldest unit of the peninsula and consist of cemented limestone, quartzite sandstones. The limestone mainly made up of reef. Then, the Lower-Middle Devonian Kartal Formation, Middle-Upper Devonian Tuzla Formation, Lower Carboniferous Baltalimanı Formation and Trace Formation deposited conformably.

Devonian aged Kartal formation rock consists of coarse limestone, limy shale, graywacke and fossilious limestone with clay interlayer. Tuzla Formation made up of fossilious limestone, calcareous shale and siliceous bedded rock.

Carboniferous aged rock unit, which are located at upper levels of Paleozoic Basement and occurred mostly at the western side of the Bosphorous. Carboniferous sequence starts with its bottom unit of Baltalimanı Formation over Tuzla Formation. Baltalimanı Formation consists of lydites and siliceous shale bounded by nodular limestone and/or graywacke at the base and partly calcareous shale at the top. This slightly thin unit outcrops at a narrow belt. The typical composite section is derived from Baltalimanı Creek. The lydites are dark gray to black, thinly laminated and form sedimentation unit average 4 cm in thickness. The unit includes a prolific radiolarian micrafauna (Kaya, 1973). Then Trace formation deposited on Baltalimanı formation conformably. Trace Formation is a succession of shale, siltstone, graywacke, sandstone subordinate conglomerate and carbonates, bounded by lydites at the base and limestone at the top. A regional tectonism and related regression accompanies to erosion of Paleozoic sequence. Hercynian orogeny of Late Paleozoic resulted in regional uplift and erosion of Paleozoic rocks.

Tertiary sediments lying with angular unconformably on Paleozoic formations start with Kırklareli formation, the deposition of which continued from Middle Eocene through Early Oligocene. The sequence starts transgressively with a basal conglomerate and levels containing clay and coal, which are fallowed by cream limy claystone and karstic reef limestone. The sequence ends with lithologies such as argillaceous limestone, marl and limy sandstone. On top of this unit, Gürpinar, Çamurluhan, Çukurçeşme, Güngören and Bakırköy Formations, a new phase of deposition, commencing again with layers of gravel, sand and coal, took place till the end of Miocene . The sand and gravel layers often encountered in the bottom levels of Gürpınar are gradually followed by overconcolidated

green clay which is frequently interbedded with sand. Çamurluhan Formation conformably overlies Gürpınar formation in a very restricted area, especially north of Bayrampaşa, south of Atışalanı köyü and southwest of Gaziosmanpaşa . Çamurluhan Formation consists of gravel, sand, clay with sand interlayer, marl, weak sandstone. Çukurçeşme Formation overlies conformably Gürpınar clay but unconformably Trace Formation. It is made up of gray, grayish white fossilius sand and gravel with greenish brown clay and marl interlayers. Güngören Formation is situated as gradually passing up from Çukurçeşme unit of the sedimentary bottom and passes up to overlying Bakırköy limestone. Güngören Formation is dominantly grayish green colored having silt and fine sand bands or chalky limestone interbedings, locally contains carbonate lumps. It's thickness change between 10 and 20 meters. Bakırköy Formation comprises white, gray limestone with green, thin clay layer. Clay, limestone interbedding can be observed at the lowermost levels of the sequence.

The Pliocene aged Belgrad Formation deposits lie unconformably on older units. It is made up reddish yellow clay, silt, grayish silt and fine sand. Quaternary represented by stream sediments consisting of gravel, sand and clay. It is well developed in Istanbul Peninsula covering basements of valleys from small rivers to large depression areas.

2.2.3. Local Geology

South and west of the subject site surfaced by sandstone, siltstone, mudstone and Carboniferous aged interlayers of them belonging to Thrace Formation which are also surfacing the wide areas of West Istanbul. At the surface and upper elevations, generally Thrace Formation composed of mudstone and occasionally sandstone that are brown, very-completely weathered, fractured-closely jointed, joints are filled with clay and silt, roughly surfaced and weak-very weak in strength. At the lower elevations, mainly grey, moderately weathered, moderately-closely jointed, joints are filled with clay, moderately strong siltstone, mudstone and sandstone exists.

At the North, East, occasionally West and at middle of the subject site, wide, high plains are surfaced by Pliocene aged Belgrad Formation. Belgrad Formations covers Thrace formation discordantly. Belgrad Formation composed of reddish yellow,

occasionally grey, gravel, sand, silt and clay. Clay, silt and sand litologies of Belgrade Formation having thicknesses varying 1.50m to 21.0m have encountered at the boreholes SK-1, SK-2, SK-3, SK-4, SK-5, SK-9, SK-10, SK-13, SK-14, SK-15, SK-16, SK-17, SK-18. Below these units, rock formation belonging to Thrace formation exists. During boreholes SK-17 and SK-18, fracture surfaces of mudstone and sandstone belonging to Thrace Formation that are lying under Pliocene aged sediments are observed to be polished and the possibility of existence of slippage surfaces is determined.

Quaternar aged alluvium having limited thickness exists within the subject site in East-West and SouthEast-NorthEast orientations at bases of the valleys. However, they are not located below the subject blocks. During the geological observations alluvium unit is determined to be composed of brown-grey sand,clay and silt.

TCR, RQD and SCR values of Trace formation are shown on the borehole logs, and the values present high amount variations related to the fractured structure of mudstone and sandstone formations. After completion of the boreholes, ground water measurements were performed. As shown in Table 2.2, ground water table has encountered with the 2.0m to 10.50m depths from the ground surface. At the boreholes performed at the Thrace Formation, the encountered groundwater is leakage of surface water from the fractures of rocks rather than a phreatic surface of an aquifer.

Table 2.3. Soil mechanics laboratory test results

Boring No	Specimen No	Depth (m)	Water Content wn (%)	Atterberg's Limits			Sieve Analysis		Classification USCS
				LL	PL	PI	+No.4 (%)	-No.200 (%)	
				36	17	19	0	79	CL
SK-4	SPT-2	3.00-3.45	23	73	31	42	0	100	CH
	SPT-5	7.50-7.95	24	44	21	23	0	87	CL
	SPT-8	12.00-12.45	21	40	NP	NP	0	74	ML
A5 SK-1	CORE-3	6.00-7.50	-	36	16	20	0	51	CL
A5 SK-3	CORE-1	2.28-3.00	-	43	23	20	0.4	95	CL
SK-5	SPT-2	3.00-3.45	28	43	22	11	0	84	ML
	SPT-5	7.50-7.95	20	37	NP	NP	0	78	CL

Not/Note: +No.4(%) : percentage material retained on No. 4 sieve /
-No.200(%) : percentage material passing the No. 200 sieve /
LL(%) : Liquid limit, percentage, % PI(%) : Plasticity index, percentage
PL(%) : Plastic limit, percentage, % USCS United Soil Classification System

One of the single most important factors affecting SPT results is the energy delivered to the SPT sampler. This is normally expressed in terms of the rod energy ratio (ER). An energy ratio of 60 per cent has generally been accepted as the reference value, which represents the approximate historical average SPT energy. The value of ER (per cent) delivered by a particular SPT set-up depends primarily on the type of the hammer/anvil system and the method of hammer release. Values of the correction factor to modify the SPT results to 60 per cent energy (ER/60) can vary from 0.3 to 1.6 corresponding to field values of ER of 20 per cent to 100 per cent. Additional correction factors are also required for rod lengths less than 10 m, borehole diameters outside the recommended interval (65–125 mm) and samplers without internal liners. Since the SPT N value also varies with the effective overburden stress level, an overburden stress correction factor is usually also applied to provide a consistent reference (i.e. $(N_1)_{60}$). Therefore the obtained SPT N values during the course of boreholes are corrected for overburden stress, rod length, borehole diameter and sampling method is given by:

$$(N_1)_{60} = N\, C_N\, C_E\, C_B\, C_R\, C_S \tag{2.1}$$

where N is the measured SPT blow count; $C_N = (P_a/\sigma'_{vo})^{0.5}$ (with a restriction that $C_N<1.7$) is a correction for effective overburden stress; C_E=ER/60% is correction to account for rod energy; ER is the actual energy ratio, in percent; C_B is correction for borehole diameter; C_R is a correction for rod length; and C_S is a correction for the sampling method. Correction factors are given in Table 2.4.

Table 2.4. Correction factors

Factor	Equipment Variable	Term	Correction
Overburden Pressure		C_N	$(P_a/\sigma'_{vo})^{0.5}$ but $C_N \leq 1.7$
Energy Ratio	Donut Hammer Safety Hammer Automatic Hammer	C_E	0.5 to 1.0 0.7 to 1.2 0.8 to 1.3
Borehole Diameter	65 mm to 115 150 mm 200 mm	C_B	1.0 1.05 1.15
Rod Length	0 to 3 m 3 m to 4 m 4 m to 6 m 6 m to 10 m 10 m to 30 m > 30 m	C_R	0.75 0.80 0.85 0.95 1.0 <1.0
Sampling Method	Standard Sampler Sampler without liner	C_S	1.0 1.1 to 1.3

In Figure 2.7 and Figure 2.8, SPT/N values (corrected for energy), obtained from standard penetration tests, are given plotted against depth. As it can be seen from both figures, in the fill layer SPT/N blow counts varies between N=2 and N=+50 and generally has homogenous consistency. Upper section of the existing Belgrad clay formation is considered as stiff-very stiff with respect to SPT/N blow counts. Lower section of the existing clay formation is considered as hard with respect to SPT/N blow counts (N>30+).

Based on the soil investigations geotechnical modeling of the site is developed and shown in Figure 2.9. Foundation elevation for A4 is located on Belgrad Formation, on the other hand, for A5 is located on weathered Trace Formation. When the super structure limited settlement criteria and loads are taken into account, a deep foundation system need was realized.

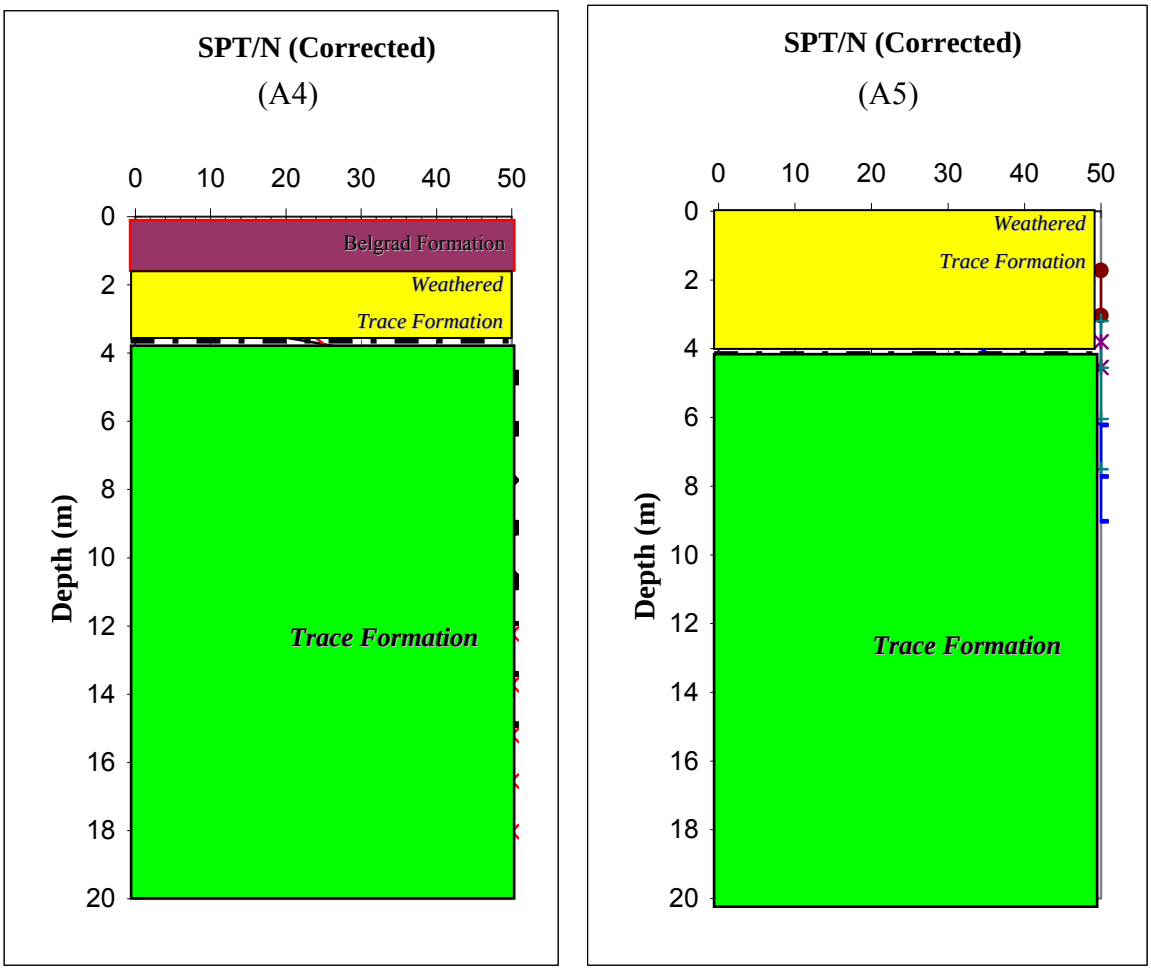

Figure 2.7. Change of SPT/N with respect to depth for A4 and A5 blocks.

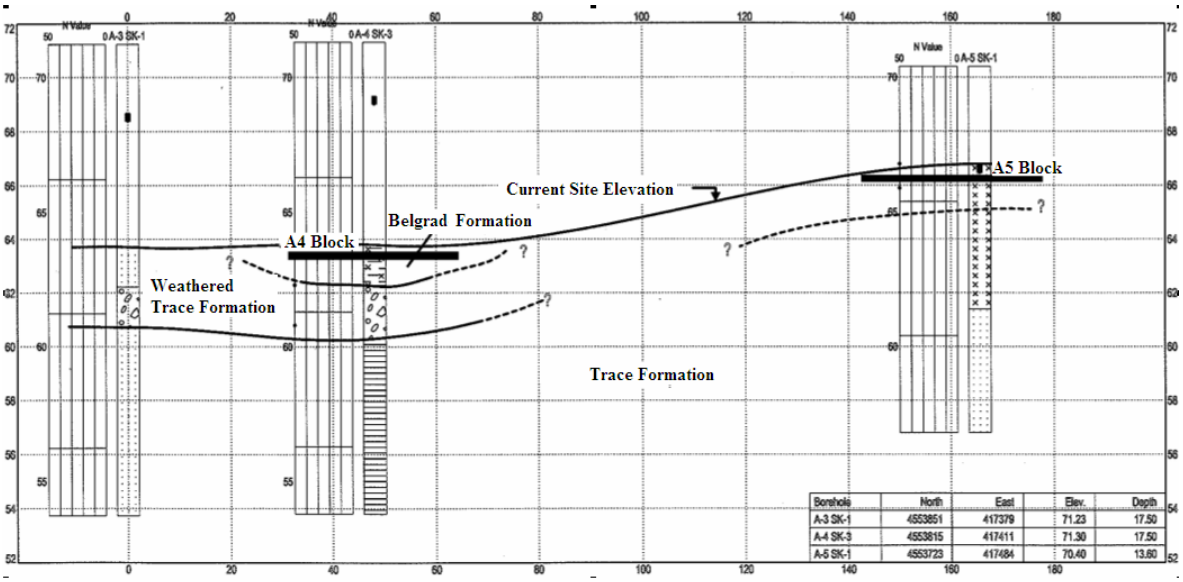

Figure 2.8. Geotechnical modeling of the site

3. VERTICAL DESIGN LOAD OF PILES AND PILE DESIGN

3.1. Introduction

When an axially loaded drilled shaft in rock medium is designed, the calculation usually involves computation of ultimate load capacity and prediction of vertical displacement under working load. The determination of the ultimate load capacity will be discussed in this chapter. Axially loaded drilled shafts in rock are designed to transfer structural loads to rock in one of the following ways (CGS, 1985): by side shear, by end bearing and combination of side shear and end bearing.

Situations where support is provided only by side shear, resistance are those where the base of the drilled hole cannot be cleaned so that it is uncertain if any end bearing resistance will be developed. Furthermore, where the vertical displacements are needed to be small only, side resistance is considered. In addition, where sound bedrock underlies low strength overburden material, it may be possible to achieve the required support in end bearing only, and assume that no side shear support is developed in the overburden. However, where the shaft is drilled some depth into sound rock, a combination of side shear resistance and end bearing resistance can be assumed (Kulhawy & Goodman, 1980). One of the smaller of these values determines the load bearing capacity of a drilled shaft in rock: The ability of the rock to support the loads transferred by the shaft and the structural strength of the shaft itself.

3.2. Capacity of Drilled Shafts in Rock

When the shaft itself is assumed strong enough, its load capacity depends on the capacity of the rock to accept without distress the loads transmitted from the shaft. The required area of shaft-rock interface (i.e., the size of drilled shaft) depends on this factor. The ultimate axial load of a drilled shaft related to rock, Q_u, consists of the ultimate side shear load, Q_{us}, and the ultimate end bearing load, Q_{ub} (see Figure 3.1)

$$Q_u = Q_{us} + Q_{ub} \tag{3.1}$$

The ultimate side shear load and the ultimate end bearing load are respectively calculated as the average side shear resistance multiplied by the shaft side surface area and as the end bearing resistance multiplied by the shaft bottom area, i.e. where L and B are respectively the length and diameter of the shaft; and τ_{max} and q_{max} are respectively the average side shear resistance and the end bearing resistance. The ultimate side shear resistance and the end bearing resistance are usually determined based on local experience and building codes, empirical relations, or field load tests.

$$Q_{us} = \pi B L \tau_{\max} \tag{3.2}$$

$$Q_{ub} = \frac{\pi B^2 q_{\max}}{4} \tag{3.3}$$

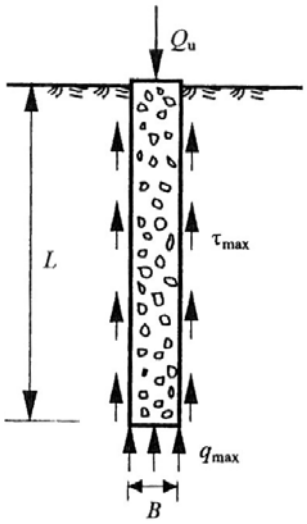

Figure 3.1. Axially loaded drilled shaft

3.2.1. Side Shear Resistance

Many factors affect the shear resistance mobilized at the shaft-rock interface. These parameters are the shaft roughness, strength and deformation properties of the concrete and the rock mass, geometry of the shaft, and initial stresses in the ground. The effect of shaft roughness is emphasized by most investigators and considered in a number of empirical relations for estimating the side shear resistance.

(a) Correlation with SPT *N* value

Standard Penetration Tests (SPT) are often carried out in weak or weathered rock. Table 3.1. shows the measured side shear resistances of drilled shafts and their corresponding SPT *N* values in weathered sedimentary rocks. It can be seen that the τ_{max}/N ratio is generally smaller than 2.0 except the case reported by Toh et al. (1989). We can also see that the τ_{max}/N ratio tends to decrease as *N* increases.

Table 3.1. Side shear resistence and SPT *N* values in weathered sedimentary rock

Rock	SPT *N* values (blows/0.3 m)	τ_{max} (kPa)	τ_{max}/N (kPa)	Reference
Highly weathered siltstone	230	>195-226	>0.87-1.0	Buttling (1986)
Highly weathered siltstone, silty sandstone and shale	100-180	100-320	1.0-1.8	Chang and Wong (1987)
Very dense clayey/sandy silt to highly weathered siltstone	110-127	80-125	0.63-1.14	Buttling and Lam (1988)
Highly to moderately weathered siltstone	200-375	340	0.9-1.7	
Completely to partly weathered interbedded sandstone, siltstone and shale/mudstone	100-150	–	1.2-3.7	Toh et al. (1989)
	150-200	–	0.6-2.3	
Highly to moderately fragmented siltstone/shale	400-1000	300-800	0.5-0.8	Radhakrishnan and Leung (1989)
Highly weathered sandy shale	150-200	120-140	0.8-0.7	Moh et al. (1993)
Slightly weathered sandy shale and sandstone	375-430	240-280	ave. 0.65	

(b) Empirical relations between side shear resistance and unconfined compressive strength of intact rock

Empirical relations between the side shear resistance and the unconfined compressive strength of rock have been proposed by many researchers. The form of empirical relations between side shear resistance and unconfined compressive strength of intact rock can be generalized as:

$$\tau_{max} = \alpha \sigma_c^{\beta} \tag{3.4}$$

where τ_{max} is the side shear resistance; σ_c is the unconfined compressive strength of the intact rock (if the intact rock is stronger than the shaft concrete, σ_c of the concrete is used); and α and β are empirical factors.

The empirical factors proposed by a number of researchers have been summarized by O'Neill et al. (1996) and are shown in Table 3.2. Most of these empirical relations were developed for specific and limited data sets, which may have correlated well with the proposed equations. However, O'Neill et ai. (1996) compared the first nine empirical relations listed in Table 3.2 with an international database of 137 pile load tests in intermediate-strength rock and concluded that none of the methods could be considered a satisfactory predictor for the database.

Table 3.2. Emprical factors α and β for side shear resistance(modified from O'Neill et al.,1996)

Design method	α	β
Horvath and Kenney (1979)	0.21	0.50
Carter and Kulhawy (1988)	0.20	0.50
Williams et al. (1980)	0.44	0.36
Rowe and Armitage (1984)	0.40	0.57
Rosenberg and Journeaux (1976)	0.34	0.51
Reynolds and Kaderbek (1980)	0.30	1.00
Gupton and Logan (1984)	0.20	1.00
Reese and O'Neill (1987)	0.15	1.00
Toh et al. (1989)	0.25	1.00
Meigh and Wolshi (1979)	0.22	0.60
Horvath (1982)	0.20 -- 0.30	0.50

Culhawy and Phoon (1993) developed a relatively extensive load test database for drilled shafts in soil and rock and presented their data both for individual shaft load tests and as site-averaged data. The results are shown in Figures 3.2 and 3.3,-in terms of adhesion factor, α_c, versus normalized shear strength, c_u/ pa or σ_c/ 2pa (assuming $c_u \approx \sigma_c / 2$), where p_a is atmospheric pressure (≈ 0.1 MPa). It should be noted that Kulhawy and Phoon (1993) defined α_c as the ratio of the side shear resistance τ_{max} to the undrained shear strength c_u. In a comprehensible manner, the results of individual load

tests show considerably greater scatter than the site-averaged data. By taking into account the site-averaged data, Kulhawy and Phoon (1993) proposed the following relations:

Table 3.3. α_c and τ_{max} relations for drilled shafts in rock (Kulhawy and Phoon, 1993)

Mean Behavior	$\alpha_c = \frac{\tau_{max}}{\sigma_c / 2} = 2.0[\sigma_c / 2p_a]^{-0.5}$
Upper Bound	$\alpha_c = \frac{\tau_{max}}{\sigma_c / 2} = 3.0[\sigma_c / 2p_a]^{-0.5}$
Lower Bound	$\alpha_c = \frac{\tau_{max}}{\sigma_c / 2} = 1.0[\sigma_c / 2p_a]^{-0.5}$

This equation can be rewritten as:

$$\alpha_c = \frac{\tau_{max}}{\sigma_c / 2} = \Psi[\sigma_c / 2p_a]^{-0.5} \tag{3.5}$$

where Ψ = 1.0 to 3.0.

This leads to a general expression for the side shear resistance:

$$\tau_{max} = \Psi[p_a \sigma_c / 2]^{-0.5} \tag{3.6}$$

It is very important to note that the empirical relations given in upper and lower bound equations are bounds to site-averaged data, and do not necessarily represent bounds to individual shaft behavior. The coefficient of determination (Ψ) is approximately 0.71 for the site-averaged data, but is only 0.46 for the individual data, reflecting the much greater variability of the individual test results (Seidel & Haberfield, 1995).

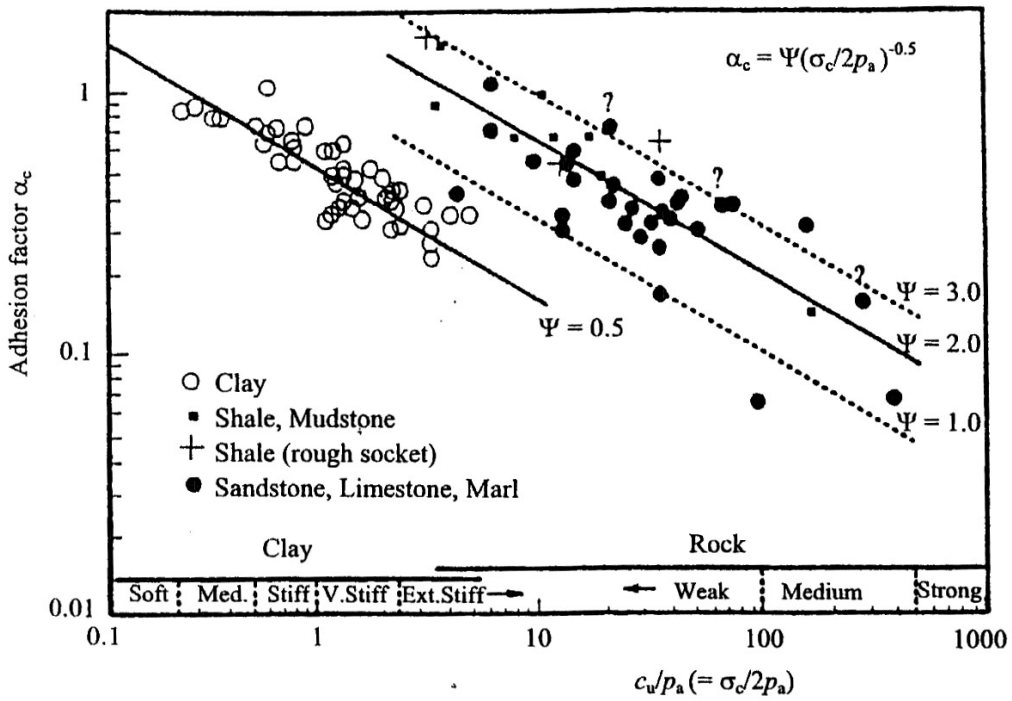

Figure 3.2. Adhesion factor α_c ($=\tau_{max}/0.5\sigma_c$) versus normalized shear strength for site-averaged data (after Kulhawy and Phoon, 1993)

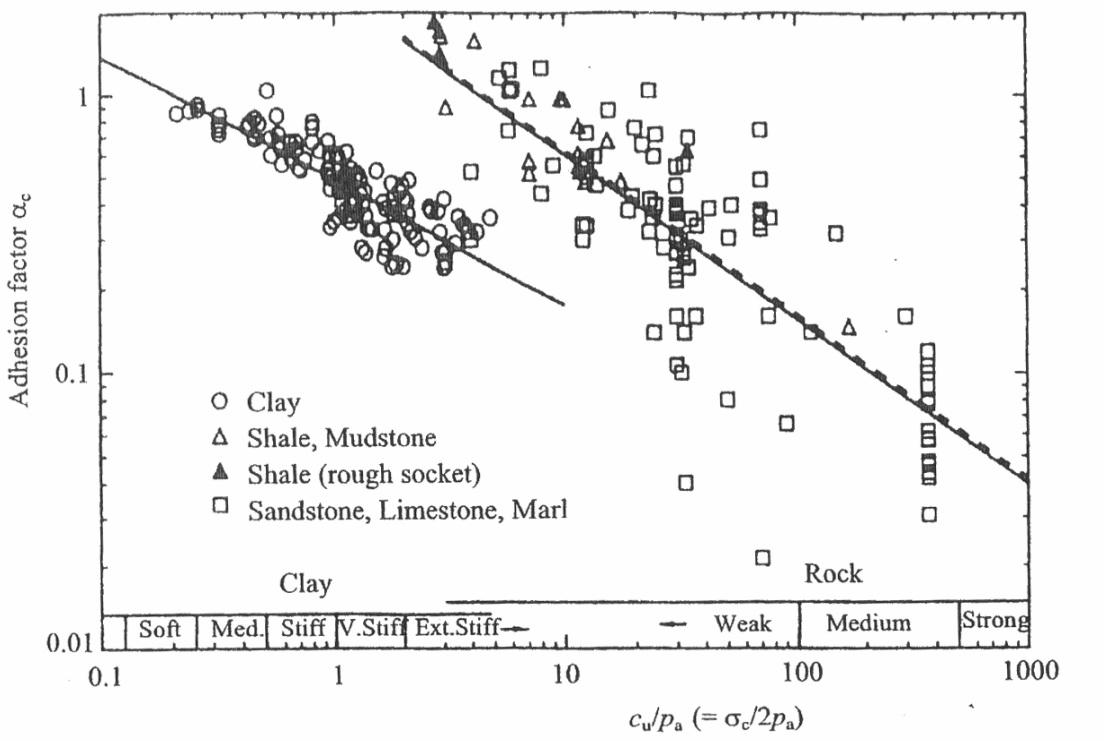

Figure 3.3. Adhesion factor α_c ($=\tau_{max}/0.5\sigma_c$) versus normalized shear strength for individual test data (after Kulhawy and Phoon, 1993)

(c) Empirical relations considering roughness of shaft wall

The roughness of the shaft wall is an important factor controlling the development of side shear resistance. Depending on the type of drilling technique and the hardness of the rock, a drilled shaft will have a certain degree of roughness. Research has shown that the benefits gained from increasing the roughness of a shaft wall can be quite significant, both in terms of peak and residual shear resistance. Studies by Williams et al. (1980) and others showed that smooth-sided shafts exhibit a brittle type of failure, while shafts having an adequate roughness exhibit ductile failure. Williams and Pells (1981) suggested that rough shafts generate a locked-in normal stress such that there is practically no distinguishing difference between peak and residual side shear resistance.

Classification of roughness proposed by Pells et al. (1980) is based on the size and frequency of grooves in the shaft wall (see Table 3.4). Based on this classification, Rowe and Armitage (1987b) proposed the following relation for shafts with different roughness:

$$\tau_{\max} = 0.45\sigma_c^{-0.5} \qquad \text{For shafts with roughness R1, R2 or R3} \tag{3.7}$$

$$\tau_{\max} = 0.60\sigma_c^{-0.5} \qquad \text{For shafts with roughness R4} \tag{3.8}$$

Horvath el al. (1980) also developed a relation from model shaft behavior using various roughness profiles. They found that as shaft profiles go from smooth to rough, the roughness factor increases significantly, as does the peak side shear resistance. These findings were confirmed in a later study by Horvath et al. (1983), and the following equation was proposed for the roughness factor (RF):

$$RF = \frac{h_m L_t}{RL} \tag{3.9}$$

where h_m is the average roughness height of the shaft; L_t is the total travel length along the shaft wall profile; R is the nominal radius of the shaft; and L is the nominal length of the shaft (see Fig. 3.4). Using Equation (3.10), the following relation was developed between the side shear resistance and RF:

Table 3.4. Roughness classes after Pells et al. (1980)

Roughness Class	Description
R1	Straight, smooth-sided shaft, grooves or indentation less than 1.00 mm deep
R2	Grooves of depth 1-4 mm, width greater than 2 mm, at spacing 50 to 200 mm.
R3	Grooves of depth 4-10 mm, width greater than 5 mm, at spacing 50 to 200 mm.
R4	Grooves or undulations of depth greater than 10 mm, width greater than 10 mm, at spacing 50 to 200 mm.

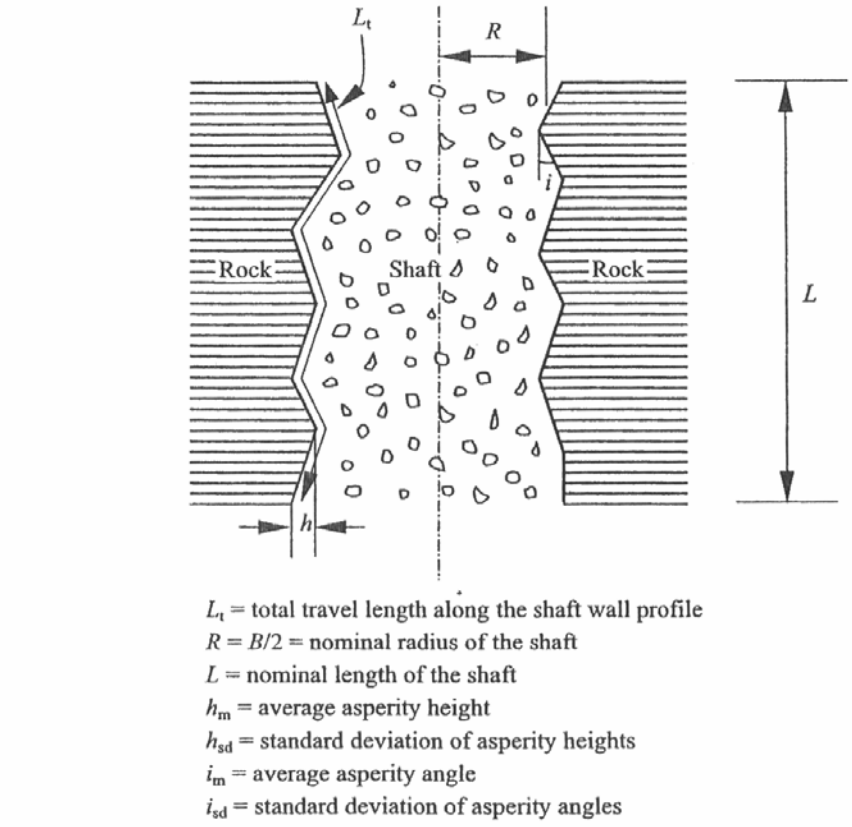

Figure 3.4. Parameters for defining shaft wall roughness (after Horvath et al.,1980 and Kodikara et al., 1992)

$$\tau_{\max} = 0.8\sigma_c \left(RF\right)^{0.45} \tag{3.10}$$

Kodikara et al. (1992) developed a rational model for predicting the relationship of τ_{max} to σ_c based on a specific definition of interface roughness, initial normal stress on the interface and the stiffness of the rock during interface dilation. The model accounts for

variability in asperity height and angularity, assuming clean, triangular interface discontinuities. Figure 3.5 shows the predicted adhesion factor, σ (τ_{max}/σ_c), for Melbourne Mudstone with the range of parameters and roughnesses as given in Table 3.5. The adhesion factor is presented as a function of E_m/σ_c, σ_c/σ_n and the degree of roughness, where E_m is the elastic modulus of the rock mass and σ_n is the initial normal stress on the shaft-rock interface. It can be seen that the adhesion factor is affected not only by the interface roughness, but also by E_m/σ_c and σ_c/σ_n.

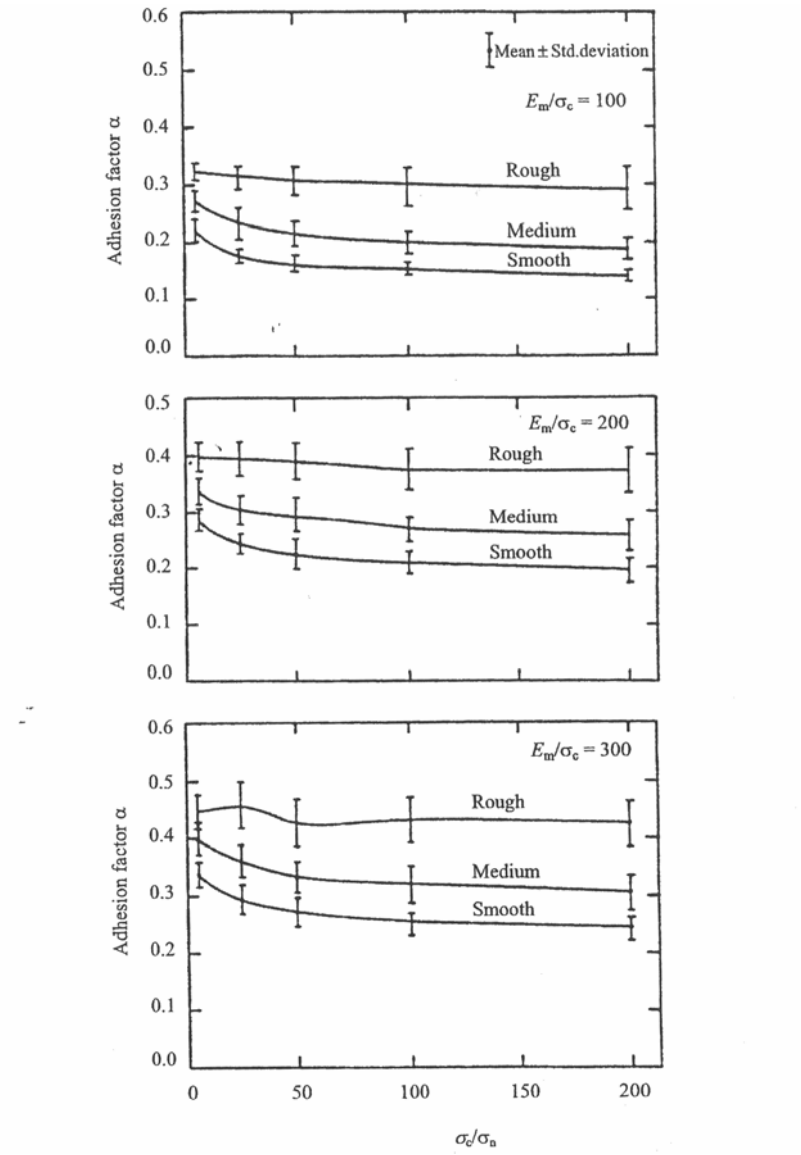

Figure 3.5. Simplified design charts for adhesion factor α (=τ_{max}/σ_c) for Melbourne Mudstone (after Kodikara et al.,1992)

Table 3.5. Definition of borehole roughness and range of parameters for Melbourne Mudstone (after Kodikara et al., 1992)

	Range of values for shafts in Melbourne Mudstone		
Parameter	Smooth	Medium	Rough
i_m (degrees)	10-12	12-17	17-30
i_{sd} (degrees)	2-4	4-6	6-8
h_m (mm)	1-4	4-20	20-80
h_{sd}/h_m		0.35	
B (m)		0.5 - 2.0	
σ_c (MPa)		0.5 - 10.0	
σ_n (MPa)		50 - 500	
E_m (MPa)		50 - 500	

Seidel and Collingwood (2001) introduced a nondimensional factor called Shaft Resistance Coefficient (SRC) to reflect the influence of shaft roughness and other factors on the shaft side shear resistance. The SRC is defined as follows:

$$SRC = \eta_c \frac{n}{1+\nu} \frac{h_m}{B} \tag{3.11}$$

where h_m is the mean roughness height; B is the shaft diameter; η_c is the construction method reduction factor as shown in Table 3.6; n is the ratio of rock mass modulus to the unconfined compressive strength of the rock (E_m/σ_c) known as the modulus ratio; and ν is the Poisson's ratio of the rock. Using SRC, Seidel and Collingwood (2001) have created shaft resistance charts as shown in Figures 3.6 and 3.7. These charts are based on results of a parametric study using a computer program called ROCKET.

(d) Estimation of roughness height of shaft wall

Application of the empirical relations considering shaft wall roughness in design requires estimation of likely shaft wall roughness height. A small number of studies have produced actual roughness profiles which enable quantitative analysis. Detailed studies have been carried out into shafts in Melbourne Mudstone (Williams, 1980; Holden, 1984; Kodikara et al., 1992; Baycan, 1996). The results show that shaft wall roughness in this low- to medium-strength argillaceous rock can vary considerably and appears to be influenced by rock discontinuities, drilling techniques, and rate of advance. Shaft wall roughness profiles in medium-strength shale were also recorded by Horvath et al. (1983),

but most of their shafts were artificially roughened by grooving. O'Neill & Hassan (1994) and O'Neill et al., (1996) recorded measurements of roughness profiles of shafts in clay shale, argillite and sandstone.

Table 3.6. Indicative construction method reduction factor η_c
(after Seidel and Collingwood, 2001)

Construction method	η_c
Construction without drilling fluid	
Best construction practice and high level of construction control (e.g., shaft sidewalls free of smear and remoulded rock)	1.0
Poor construction practice or low-quality construction control (e.g., smear or remoulded rock present on shaft sidewalls)	0.3 – 0.9
Construction under bentonite slurry	
Best construction practice and high level of construction control	0.7 – 0.9
Poor construction practice or low-quality construction control	0.3 – 0.6
Construction under polymer slurry	
Best construction practice and high level of construction control	0.9 – 1.0
Poor construction practice or low-quality construction control	0.8

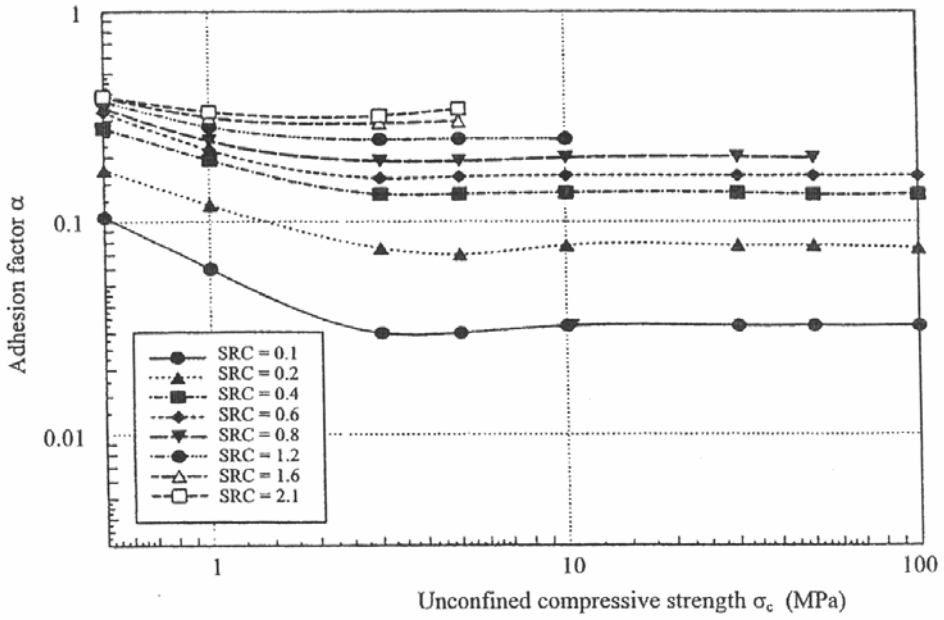

Figure 3.6. Adhesion factor α ($=\tau_{max}/\sigma_c$) versus σ_c
(after Seidel and Collingwood, 2001)

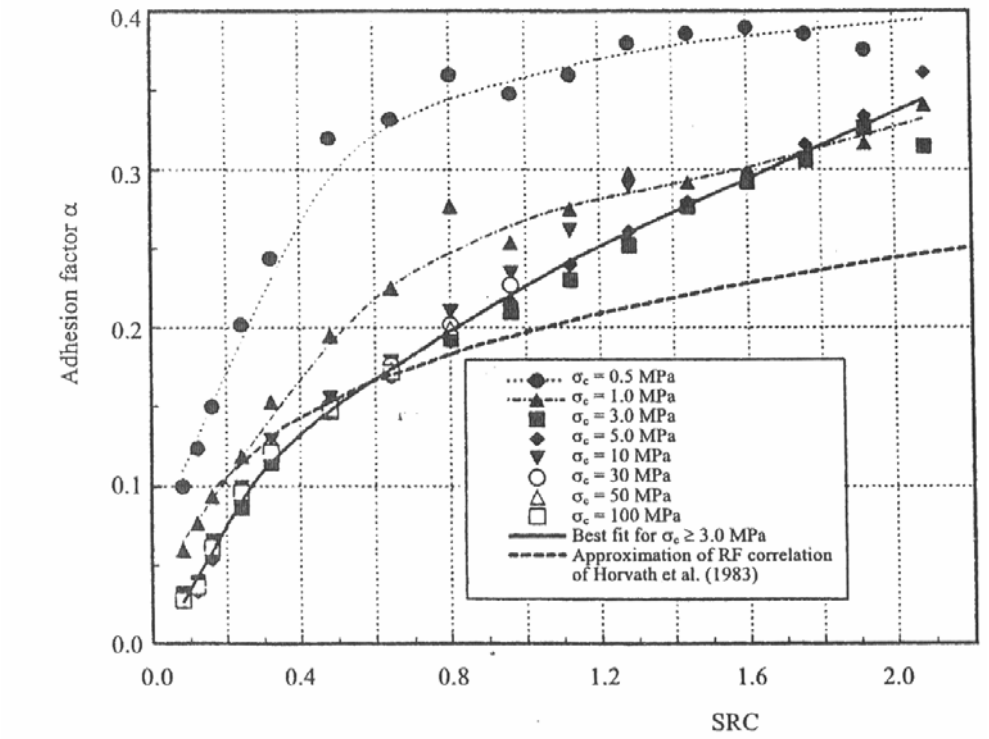

Figure 3.7. Adhesion factor α ($=\tau_{max}/\sigma_c$) versus SRC
(after Seidel and Collingwood, 2001)

Based on roughness heights back-calculaled from load tests on shafts in rock, Seidel and Collingwood (2001) developed the effective roughness height versus the unconfined compressive strength plot as shown in Figure 3.8. The back-calculations were conducted using Equation 3.11 and assuming η_c =1.0. In the case of a shaft for which the concrete-rock interface is clean and unbounded, the roughness height back-calculated assuming η_c =1.0 should provide a reasonable estimate of the roughness height magnitude. However, if the shaft resistance is adversely influenced by construction procedures, the roughness height would be underestimated if η_c is assumed to be 1.

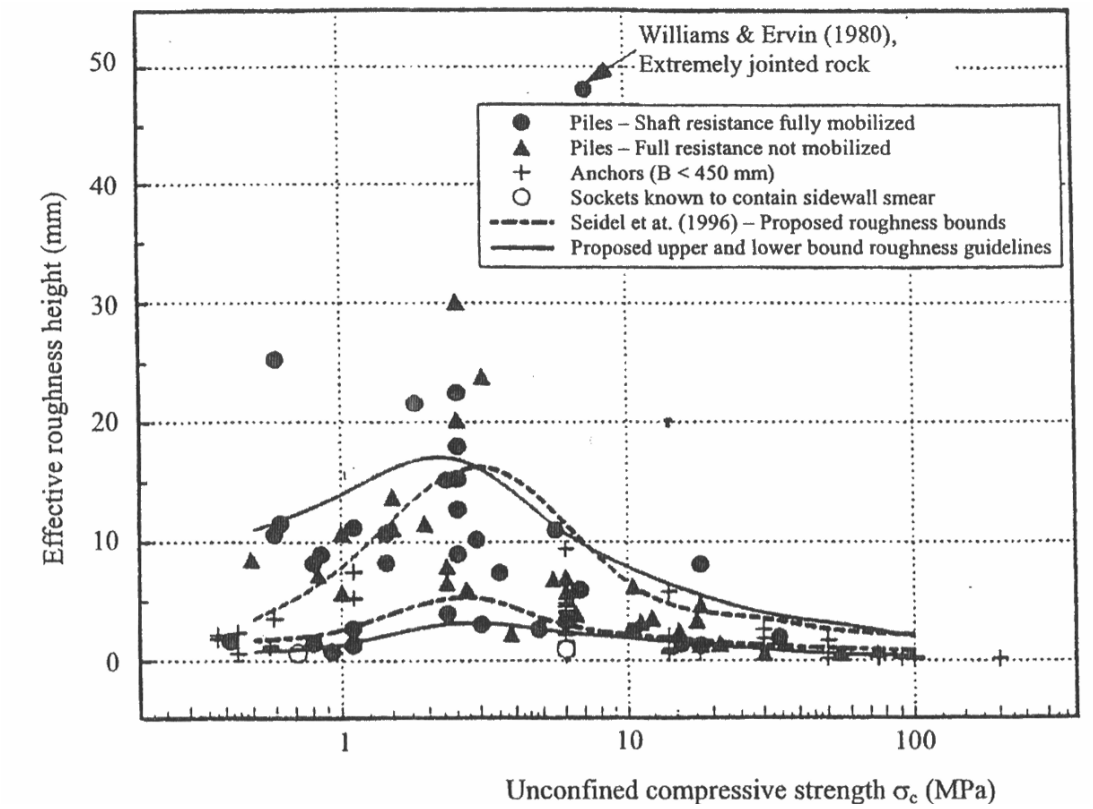

Figure 3.8. Effective roughness height versus σ_c
(after Seidel and Collingwood, 2001)

(e) Factors affecting side shear resistance

As stated above, the shaft wall roughness, which is an important factor controlling the development of side shear resistance, has been studied extensively. Other factors such as the discontinuities in the rock mass and the shaft geometry have also been studied by some researchers. Williams et al. (1980) suggested that the existence of discontinuities in the rock mass reduces the side shear resistance by reducing the normal stiffness of the rock mass. They developed the following empirical relation that considers the effect of discontinuities on the side shear resistance:

$$\tau_{\max} = \alpha_w \beta_w \sigma_c \tag{3.12}$$

where α_w is a reduction factor reflecting the strength of the rock, as shown in Figure 3.9; and β_w is the ratio of side shear resistance of jointed rock mass to side shear resistance of intact rock. β_w is a function of modulus reduction factor, j, shown in Figure 3,10, in which

$$\beta_w = f(j)$$
$$j = \frac{E_m}{E_r} \tag{3.13}$$

where E_m is the elastic modulus of the rock mass; and E_r is the elastic modulus of the intact rock. When the rock mass is such that the discontinuities are tightly closed and seams are infrequent, β_w is essentially equal to 1.0. Comparing Equation (3.12) with Equation 3.10, it can be seen that $\alpha_w\beta_w$ is just the adhesion factor, α, for β=1. Since α_w is derived from field test data, the effect of discontinuities is already included in α_w. If α_w is multiplied by β_w which is obtained from laboratory tests (Williams et al., 1980), the effect of discontinuities will be considered twice. So Equation (3.12) may be too conservative. Pabon and Nelson (1993) studied the effect of soft horizontal seams on the behavior of laboratory model shafts. The study included four instrumented model shafts in manufactured rock, three of which have soft seams. They concluded that a soft seam significantly reduces the normal interface stresses generated in the rock layer overlying it. Consequently the side shear resistance of shafts in rock with soft seams is much lower than that of shafts in intact rock.

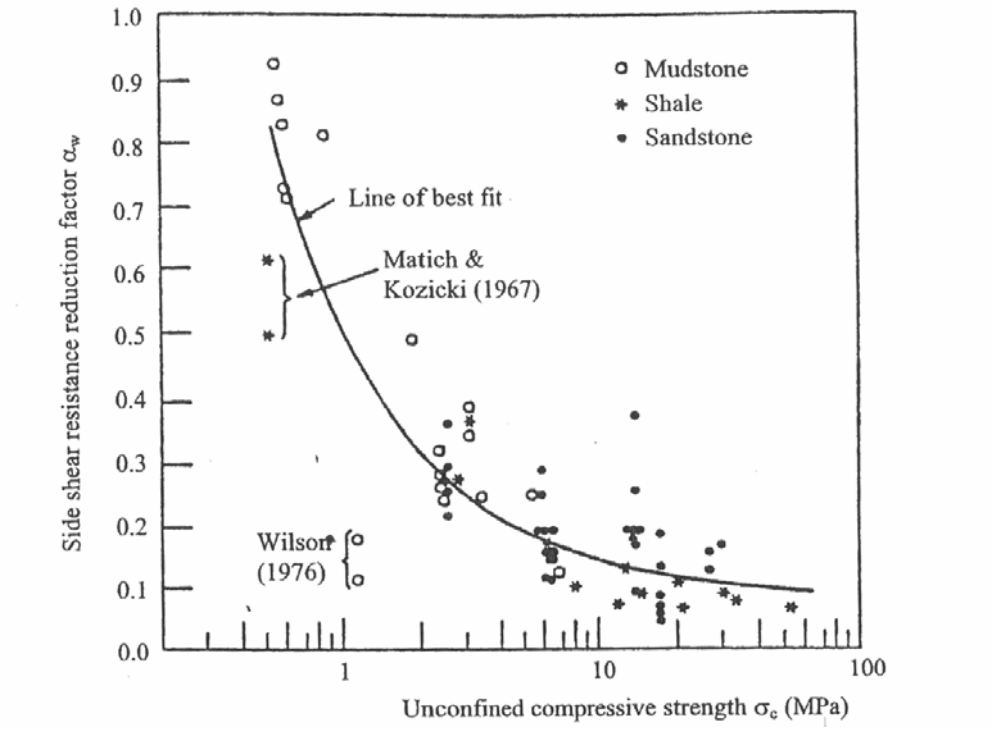

Figure 3.9. Side shear resistance reduction factor α_w (after Williams and Pells, 1981)

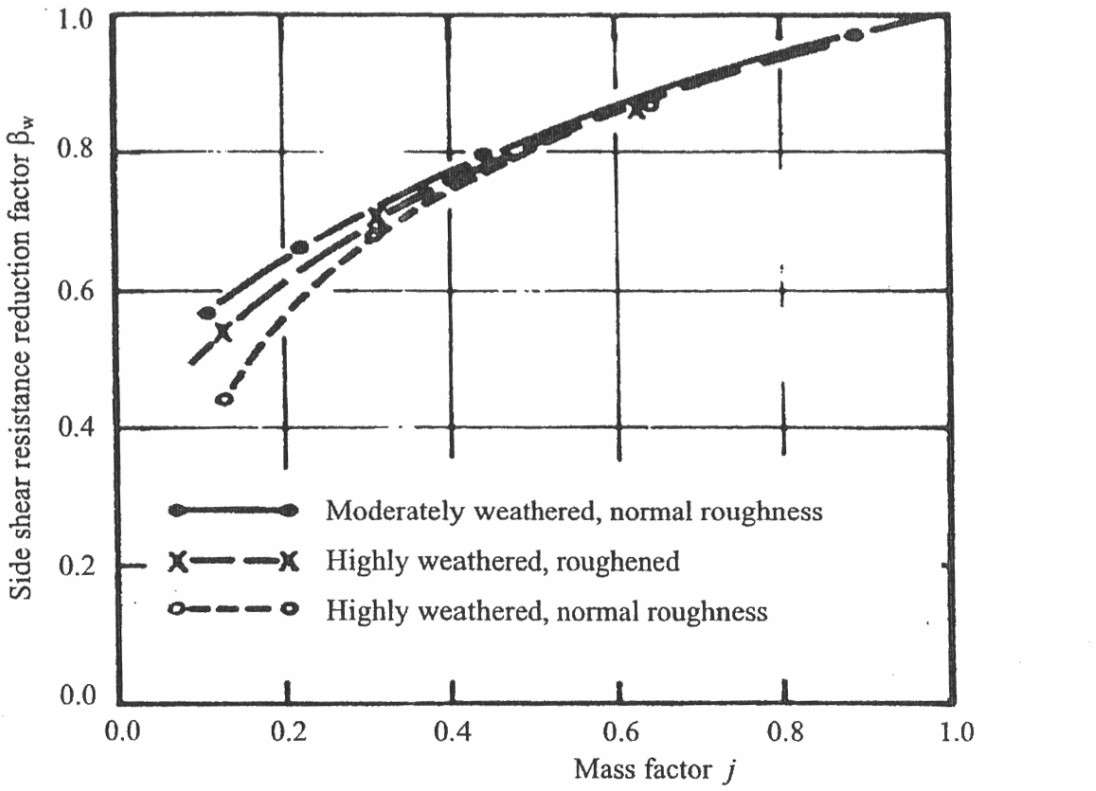

Figure 3.10. Side shear resistance reduction factor β_w (after Williams and Pells, 1981)

3.2.2. End Bearing Resistance

(a) End bearing behavior of drilled shafts

The typical bearing capacity failure modes for rock masses depend on discontinuity spacing with respect to foundation width (or diameter), discontinuity orientation, discontinuity condition (open or closed), and rock type. Table 3.7 illustrates typical failure modes according to rock mass conditions (ASCE, 1996). Prototype failure modes may actually consist of a combination of modes.

Table 3.7. Typical bearing capacity failure modes associated with various rock mass conditions (after ASCE, 1996)

Rock mass conditions			Failure	
	Joint dip	Joint spacing	Illustration	Mode
Intact	N/A	$s >> B$	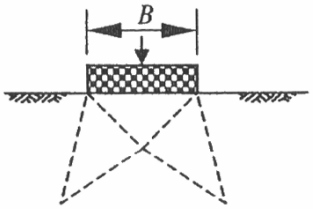	Brittle rock: Local shear failure caused by localized brittle fracture
			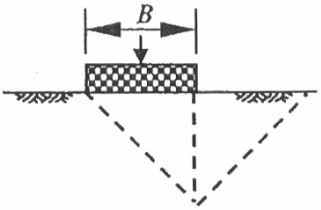	Ductile rock: General shear failure along well defined failure surfaces
Steeply dipping joints	$70° < \beta < 90°$	$s < B$	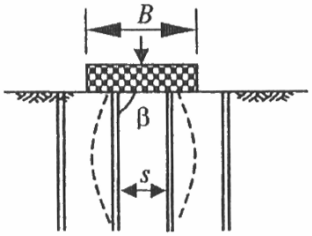	Open joints: Compressive failure of individual rock columns. Near vertical joint set(s)
			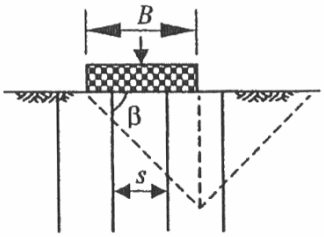	Closed joints: General shear failure along well defined failure surfaces. Near vertical joint(s)
		$s > B$	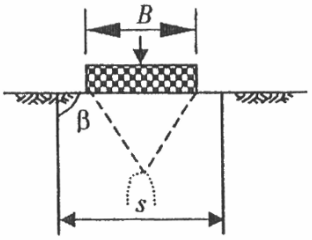	Open or closed joints: Failure initiated by splitting leading to general shear failure. Near vertical joint set(s)
Jointed	$20° < \beta < 70°$	$s < B$ or $s > B$ if failure wedge can develop along joints	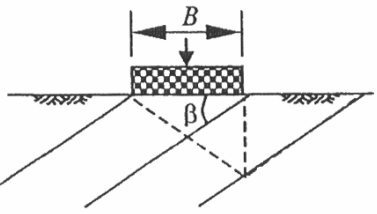	General shear failure with potential for failure along joints. Moderately dipping joint set(s)

Table 3.7. (continued) Typical bearing capacity failure modes associated with various rock mass conditions (after ASCE, 1996)

Rock mass conditions			Failure	
	Joint dip	Joint spacing	Illustration	Mode
Layered	$0° < \beta < 20°$	Limiting value of H with respect to B	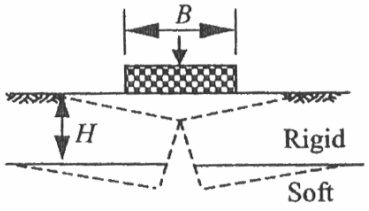	Thick rigid upper layer: Failure is initiated by tensile failure caused by flexure of the thick rigid upper layer
			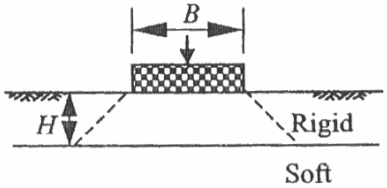	Thin rigid upper layer: Failure is initiated by punching tensile failure of the thin rigid upper layer
Fractured	N/A	$s << B$	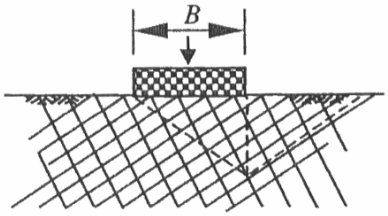	General shear failure with irregular failure surface through rock mass. Two or more closely spaced joint sets

(b) End bearing resistance based on local experience and codes

Peck et al. (1974) suggested a correlation between the allowable bearing pressure and RQD for footings supported on level surfaces in competent rock (Fig. 3.11). This correlation can be used as a first crude step in determination of the end bearing resistance of drilled shafts in rock. It need be noted that this correlation is intended only for unweathered jointed rock where the discontinuities are generally tight. If the value of allowable pressure exceeds the unconfined compressive strength ot intacl rock, the allowable pressure is taken as the unconfmed compressive strength. In Hong Kong design practice, for large diameter drilled shafts in granitic and volcanic rocks, the allowable end bearing resistance may be used as specified in Table 3.8. The presumptive end bearing resistance values range from 3.0 to 7.5 MPa, depending on the rock category which is defined in terms of the rock decomposition grade, strength and total core recovery.

The Standard Specifications for Highway Bridges adopted by the American Association of State Highway and Transportation Officials (AASHTO, 1989) also provide presumptive allowable bearing pressures for spread footing foundations in rock. These presumptive values can be used as a first crude step in determination of the end bearing resistance of drilled shafts in rock.

(c) End bearing resistance from pressuremeter test results

The Canadian Foundation Engineering Manual (CGS, 1985) proposed a method for determining the end bearing resistance of drilled shafts based on in situ pressuremeter test results:

$$q_{\max} = K_b\left(p_l - p_o\right) + \sigma_o \tag{3.14}$$

where p_l is the limit pressure as determined from pressuremeter tests in the zone extending two shaft diameters above and below the shaft base; p_o is the at rest horizontal stress in the rock at the elevation of the shaft base; σ_o is the total overburden stress at elevation of the shaft base; and K_b is an empirical non-dimensional coefficient, which depends on the depth and shaft diameter ratio as shown in Table 3.9.

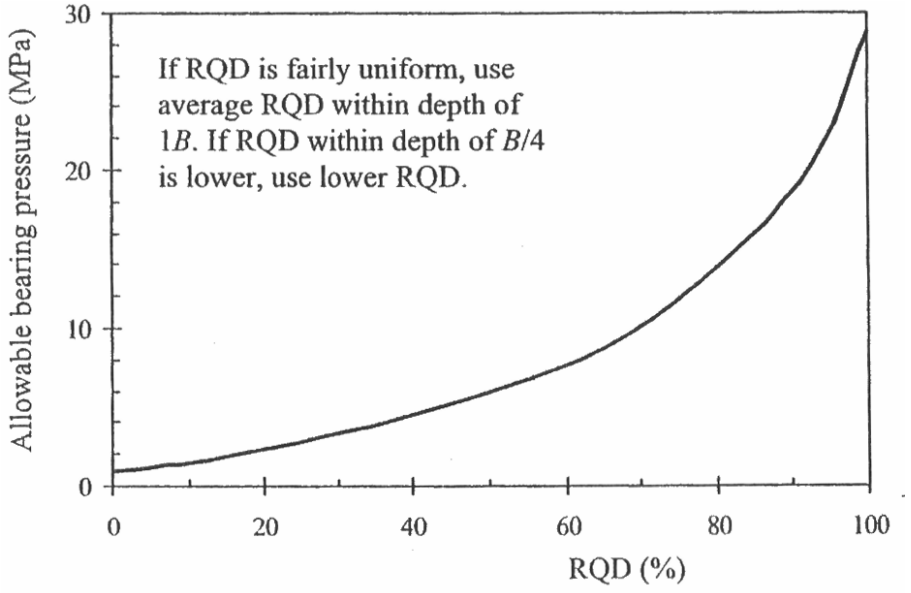

Figure 3.11. Allowable bearing pressure of jointed rock (after Peck et al.,1974)

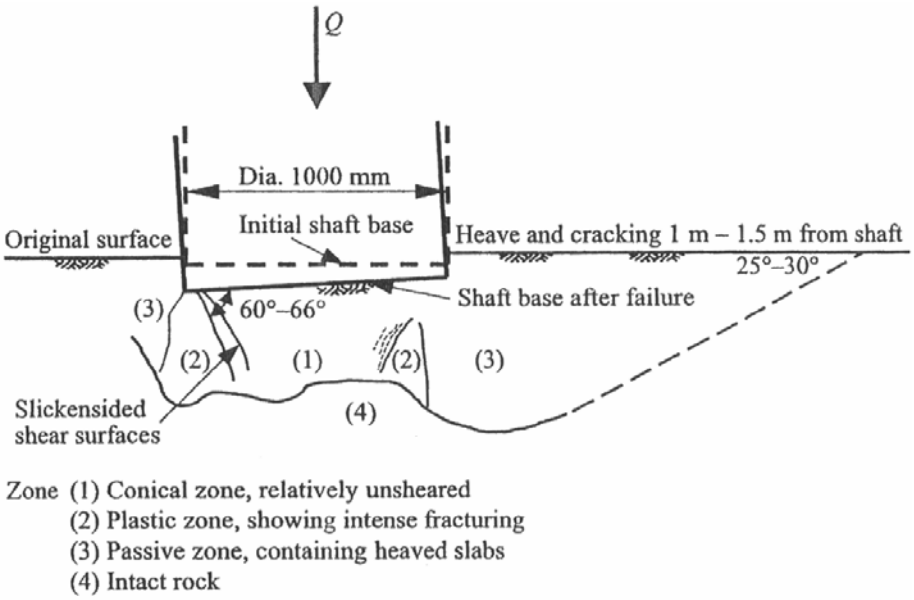

Figure 3.12. Typical failure mechanism for end bearing shafts: Base of shaft bearing at ground surface (after Williams et al., 1980)

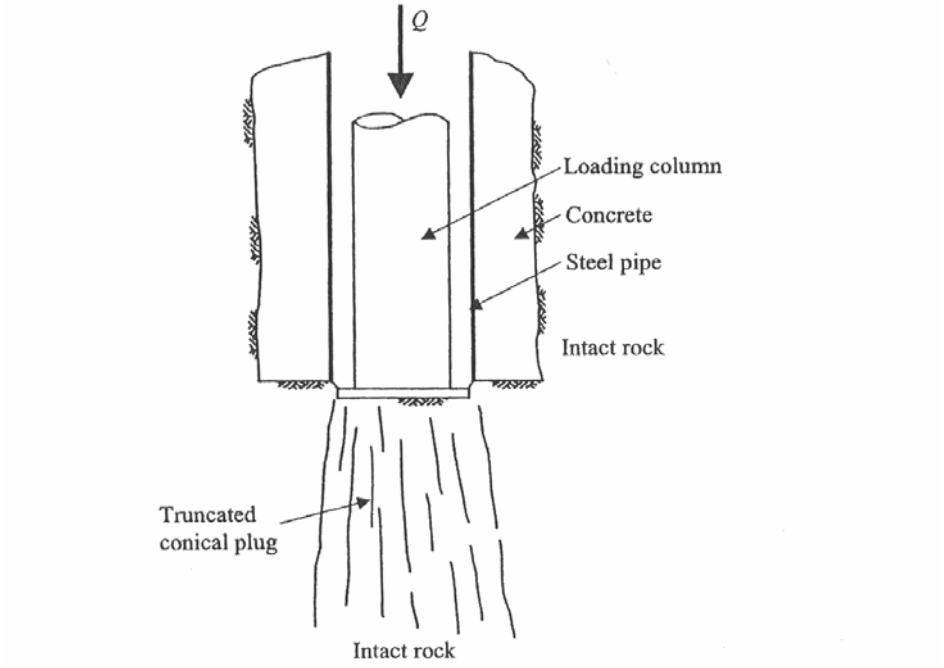

Figure 3.13. Typical failure mechanism for end bearing shafts: Shaft with length/diameter>2 (after Williams et al., 1980)

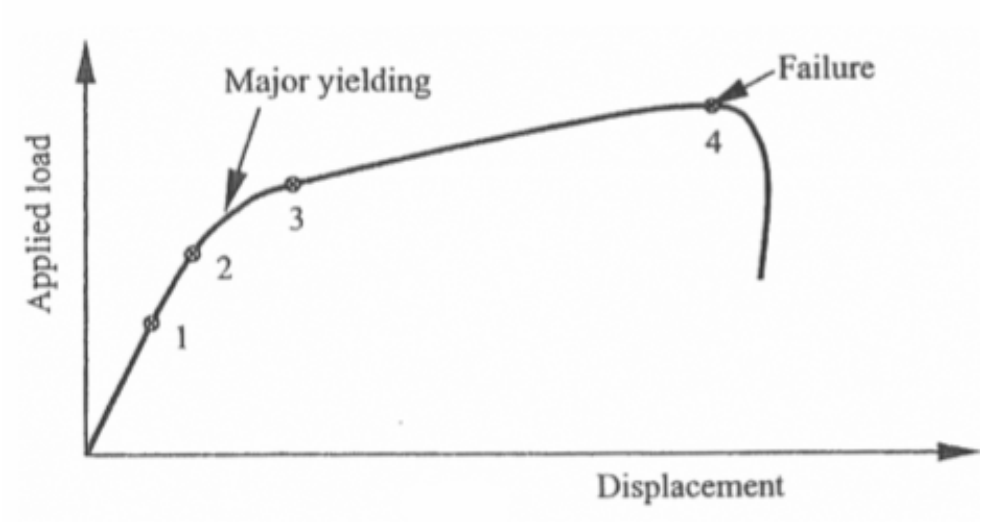

Figure 3.14. Observed progressive failure modes: Typical load-displacement curve (after Johnston and Choi, 1985)

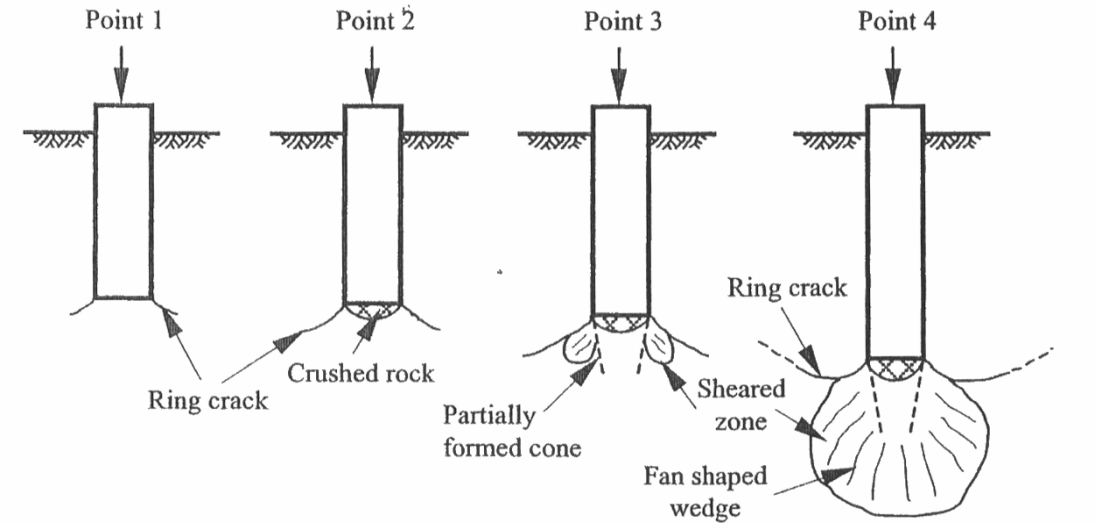

Figure 3.15. Observed progressive failure modes: Failure modes corresponding to the points in (Figure 3.13) (after Johnston and Choi, 1985)

Table 3.8. Presumed sade vertical bearing stress for foundations on horizontal ground in Hong Kong [simplified from PNAP 141 (BOO, 1990)

Category	Granitic and volcanic rock	Presumed bearing stress (MPa)
1(a)	Fresh to slightly decomposed strong rock of material weathering grade II or better, with total core recovery > 95 and minimum uniaxial compressive strength of rock material σ_c not less than 50 MPa (equivalent point load index strength PLI_{50}[a] not less than 2 MPa)	7.5
1(b)	Slightly to moderately decomposed moderately strong rock of material weathering grade II or III or better, with total core recovery > 85% and minimum unconfined compressive strength of rock material σ_c not less than 25 MPa (equivalent point load index strength PLI_{50}[a] not less than 1 MPa)	5.0
1(c)	Moderately decomposed moderately strong to moderately weak rock of material weathering grade III or IV or better, with total core recovery > 50%	3.0

[a] Point load index strength PLI_{50} of rock quoted is equivalent value for 50-mm-diameter cores (ISRM, 1979a).

(d) Empirical and Semi-Empirical Relations

Unlike the side shear resistance, numerous theories have been proposed for estimating the end bearing resistance. According to Pells and Turner (1980), the theoretical approaches fall into three categories:

1. Methods which assume rock failure to be plastic.
2. Methods which idealize the zone of failure beneath the base in a form which allows either the brittleness strength ratio or the brittleness modulus ratio to be taken into account.
3. Methods based on limiting the maximum stress beneath the loaded area to a value less than required to initiate fracture. These methods assume essentially that once the maximum strength is exceeded at any point in a brittle material, total collapse will occur.

There is a significant variation in the end bearing resistance predicted from different theories. For example, the predicted end bearing capacity of rock with an internal friction angle $\varphi = 45°$ ranges from $4.9\sigma_c$ using the incipient failure theory (Category 3) based on the modified Griffith theory to $56\sigma_c$ using the classical plasticity theory (Category 1), where σ_c is the unconflned compressive strength of intact rock (Poulos and Davis, 1980).

Because of the wide variation of theoretical results, empirical and Semi-empirical relations have been developed. Since they are more commonly used than the theoretical methods, only the empirical and semi-empirical relations are discussed in the following.

Table 3.9. K_b as function of depth and shaft diameter ratio (CGS, 1985)

Depth/Diameter	0	1	2	3	5	7
K_b	0.8	2.8	3.6	4.2	4.9	5.2

Table 3.10. Presumptive allowable bearing pressures for spread footing foundations, modified after Navy (1982) (simplified from AASHTO, 1989).

Type of bearing material	Consistency in place	Range of σ_c (MPa)	Allowable bearing pressure (MPa)	
			Ordinary range	Recommended value for use
Massive crystalline igneous and metamorphic rock: granite, diorite, basalt, gneiss, thoroughly cemented conglomerate (sound condition allows minor cracks)	Very hard, sound rock	> 250	6 – 10	8
Foliated metamorphic rock: slate, schist (sound condition allows minor cracks)	Hard sound rock	100 – 250	3 – 4	3.5
Sedimentary rock: hard cemented shales, siltstone, sandstone, limestone without cavaties	Hard sound rock	50 – 100	1.5 – 2.5	2
Weathered or broken bedrock of any kind except highly argillaceous rock (shale)	Medium hard rock	25 – 50	0.8 – 1.2	1
Compaction shale or other highly argillaceous rock in sound condition	Medium hard rock	25 – 50	0.8 – 1.2	1

In Table 3.9 there are some important points which are to be considered:

1. Variations of allowable bearing pressure for size, depth, and arrangement of footings must be determined by analysis.
2. Presumptive values for allowable bearing pressures obtained from building codes and charts developed by various agencies based on local experience with satisfactory and unsatisfactory performance; usually the pressure that will limit

total and differential settlements to 1 inch. Presumptive values arc not based on thorough engineering analysis.

3. Allowable bearing pressure for rock is controlled by rock mass discontinuities, and should not exceed the unconfined compressive strength.

Analogous to the side shear resistance, many attempts have been made to correlate the end bearing capacity, q_{max}, to the unconfined compressive strength, σ_c, of intact rock. Here are some suggested relations:

Table 3.11. q_{max} and σ_c relations

Coates(1967):	$q_{\max} = 3.0\sigma_c$	(3.15)
Rowe and Armitage (1987b):	$q_{\max} = 2.7\sigma_c$	(3.16)
ARGEMA (I992)	$q_{\max} = 4.5\sigma_c \le 10Mp$	(3.17)
Findlay et al. (1997)	$q_{\max} = (1-4.5)\sigma_c$	(3.18)

The bearing capacity of foundations on rock is largely dependent on the strength of the rock mass. Discontinuities can have a significant influence on the strength of the rock mass depending on their orientation and the nature of material within discontinuities (Pells and Turner, 1980). As.a result, relations have been developed to account for the influence of discontinuities in the rock mass. The Standard Specifications for Highway Bridges adopted by the American Association of State Highway and Transportation Officials (AASHTO, 1989) suggests that the end bearing capacity be estimated using the following relationship:

$$q_{\max} = N_{ms}\sigma_c \tag{3.19}$$

where N_{ms} is a coefficient relating q_{max} to σ_c. The value of N_{ms} is a function of rock mass quality and rock type (Table 6.11), where rock mass quality, in essence, expresses the degree of jointing and weathering. Rock mass quality has a much stronger effect on N_{ms} than rock type. For a given rock type, N_{ms} for excellent rock mass quality is more than 250

times higher than N_{ms} for poor quality. For a given rock mass quality, however, N_{ms} changes little with rock type. For example, for a rock mass of very good quality, the values of N_{ms} are 1.4, 1.6, 1.9, 2.0 and 2.3 respectively for rock types A, B, "C, D and E (see Table 3.13). It should be noted however that rock type is implicitly related to the unconflned compressive strength. Equation (3.19) may tbus represent a non-linear relation between q_{max} and σ_c. Although it is not explicitly mentioned in AASHTO (1989), Equation (3.19) and coefficient N_{ms} can be simply derived from the lower bound solution suggested by Carter and Kulhawy (1988) (see Fig. 3.16):

$$q_{\max} = \left[s^{0.5} + \left(m_b s^{0.5} + s \right)^{0.5} \right] \sigma_c \tag{3.20}$$

in which the expression in the brackets is simply the coefficient N_{ms} in Equation (3.19); and m_b and s are the strength parameters for the Hoek-Brown strength criterion. Values of m_b and s for the rock categories in Table 3.13 are shown in Table 3.14. The values of N_{ms} in Table 3.13 can be simply obtained by inserting the corresponding values of mb and s from Table 3.14 in the expression in the brackets of Equation (3.20). Zhang and Einstein (1998a) derived an expression for the end bearing capacity that considers the influence of the overburden stress (Figure 3.17):

$$q_{\max} = \left(m_b \frac{\sigma'_{IB}}{\sigma_c} + s \right)^{0.5} \sigma_c + \sigma'_{IB} \tag{3.21}$$

$$\sigma'_{IB} = \left(m_b \frac{q_s}{\sigma_c} + s \right)^{0.5} \sigma_c + q_s \tag{3.22}$$

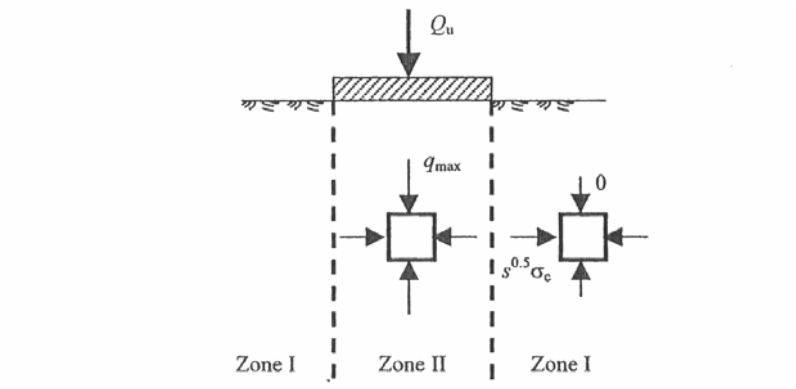

Figure 3.16. Lower-bound solution for bearing capacity (after Kulhawy and Carter, 1992)

Table 3.12. Values of N_{ms} for estimating the end bearing capacity of drilled shafts in broken or jointed rock (after AASHTO, 1989).

Rock Mass Quality	General Description	RMR[1] Rating	Q[2] Rating	RQD[3] Rating	N_{ms}[4] A	B	C	D	E
Excellent	Intact rock with joints spaced > 10 feet apart	100	500	95-100	3.8	4.3	5.0	5.2	6.1
Very Good	Tightly interlocking, undisturbed rock with rough unweathered discontinuities spaced 3 to 10 feet apart	85	100	90-95	1.4	1.6	1.9	2.0	2.3
Good	Fresh to slightly weathered rock, slightly disturbed with discontinuities spaced 3 to 10 feet apart	65	10	75-90	0.28	0.32	0.38	0.40	0.46
Fair	Rock with several sets of moderately weathered discontinuities spaced 1 to 3 feet apart	44	1	50-75	0.049	0.056	0.066	0.069	0.081
Poor	Rock with numerous weathered discontinuities spaced 1 to 20 inches apart with some gouge	23	0.1	25-50	0.015	0.016	0.019	0.020	0.024
Very Poor	Rock with numerous highly weathered discontinuities spaced < 2 inches apart	3	0.01	<25	Use q_{ult} for an equivalent soil				

(1) Geomechanics rock mass rating (RMR) system (Bieniawski, 1988) – See Chapter 2
(2) Rock mass quality (Q) system (Barton et al., 1974) – See Chapter 2
(3) Range of RQD values provided for general guidance only; actual determination of rock mass quality should be based on RMR or Q rating systems
(4) Value of N_{ms} as function of rock type; refer to Table 2.8 for typical range of values of σ_c for different rocks in each category

Table 3.13. Values of m_b and s based on rock mass classification (modified from Carter and Kulhawy, 1988).

Rock Mass Quality	General Description	RMR[1] Rating	Q[2] Rating	RQD[3] Rating	s	m_b A	B	C	D	E
Excellent	Intact rock with joints spaced > 10 feet apart	100	500	95-100	1	7	10	15	17	25
Very Good	Tightly interlocking, undisturbed rock with rough unweath-ered discontinuities spaced 3 to 10 feet apart	85	100	90-95	0.1	3.5	5	7.5	8.5	12.5
Good	Fresh to slightly weathered rock, slightly disturbed with discontinuities spaced 3 to 10 feet apart	65	10	75-90	0.004	0.7	1	1.5	1.7	2.5
Fair	Rock with several sets of moderately weathered disconti-nuities spaced 1 to 3 feet apart	44	1	50-75	10^{-4}	0.14	0.2	0.3	0.34	0.5
Poor	Rock with numerous weathered discontn-uities spaced 1 to 20 inches apart with some gouge	23	0.1	25-50	10^{-5}	0.04	0.05	0.08	0.09	0.13
Very Poor	Rock with numerous highly weathered discontinuities spac-ed < 2 inches apart	3	0.01	<25	0	0.007	0.01	0.015	0.017	0.025

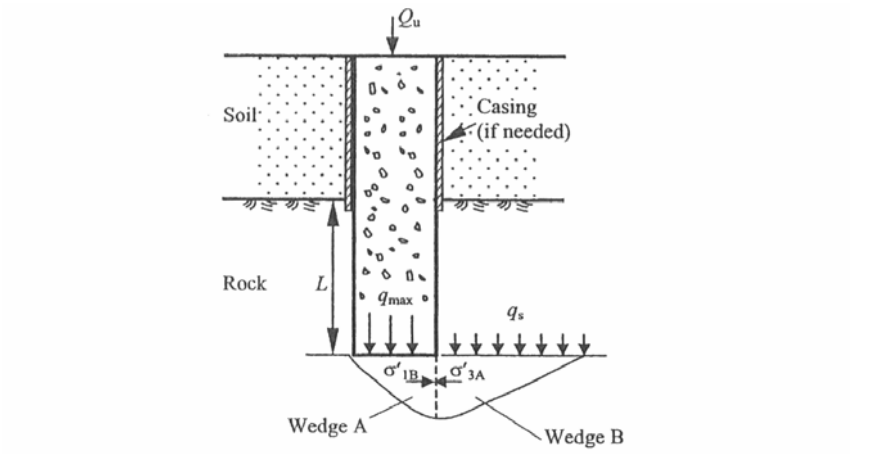

Figure 3.17. Assumed failure mode of rock mass below the shaft base (after Zhang and Einstein, 1998a)

Kulhawy and Goodman (1980) presented the following relationship originally proposed by Bishnoi (1968):

$$q_{\max} = JcN_{cr} \tag{3.23}$$

where J is a correction factor depending on normalized spacing of horizontal discontinuities; c is the cohesion of the rock mass; and N_{cr} is a modified bearing capacity factor, which is a function of the friction angle φ of the rock mass and normalized spacing of vertical discontinuities in Figure 3.19.

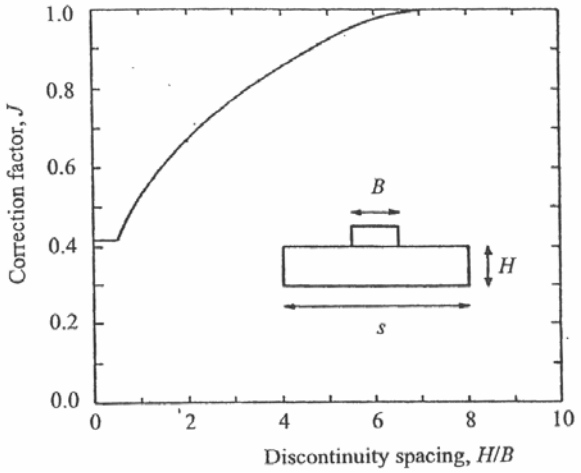

Figure 3.18. Correction factor for discontinuity spacing (after Kulhawy and Goodman, 1980)

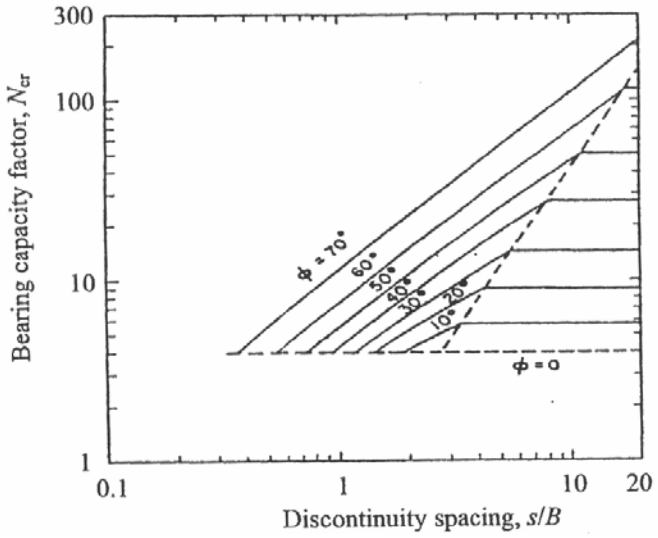

Figure 3.19. Bearing capacity factor for open discontinuties (after Kulhawy and Goodman, 1980).

As indicated in the preceding lext, the strength parameters c and φ are rock mass properties. Kulhawy and Goodman (1987) provided a table relating the rock mass properties c and φ to intact rock properties and RQD (Table 3.15).

Table 3.14. Suggested design values of strength parameters c and φ (from Kulhawy and Goodman, 1987)

RQD (%)	Rock mass properties		
	Unconfined Compressive strength	Cohesion c	Angle of friction ϕ
0 – 70	$0.33\sigma_c$	$0.1\sigma_c$	30°
70 – 100	$0.33\sigma_c - 0.8\sigma_c$	$0.1\sigma_c$	30°– 60°

σ_c = unconfined compressive strength of intact rock

The correction factor J considers the effect of horizontal discontinuities and the variation of J with the discontinuity spacing is shown in Figure 3.18, where H is the spacing of horizontal discontinuities. For the value of N_{cr} the authors considered the discontinuities being either open or closed. According to Goodman (1980), the presence of open discontinuities would allow failure to occur by splitting (because the discontinuities are open, there is no confining pressure and failure is likely to occur by uniaxial compression of the rock columns), and this mode of failure needs to be included in the calculation of the end bearing capacity. Several charts are given by Kulhawy and Goodman (1980), following the method of Bishnoi (1968), to determine N_{cr} for both open and closed discontinuities.

The Canadian Foundation Engineering Manual (CGS, 1985) proposed that the end bearing pressure be calculated using the following equation:

$$q_{\max} = 3\sigma_c K_{sp} D \tag{3.24}$$

where $K_{sp} = [3 + s/B]/\left[10 \times (1 + 300g/s)^{0.5}\right]$ is an empirical factor; s is the spacing of the discontinuities; B is the shaft width or diameter; g is the aperture of the discontinuities; $D = 1 + 0.4(L/B \le 3.4)$ is the depth factor; L is the shaft length. In general the method will

apply only if s/B ratios lie between 0.05 to 2.0 and the values of g/s between 0 and 0.02 (CGS, 1985).

Chang and Einstein (1998a) developed a database of 39 shaft load tests about the ultimate end bearing capacity (Table 3.16). This database represents rocks of relatively low strength. Table 3.16 lists, in addition to shaft dimensions, the unconfined compressive strength of intact rock σ_c, the end bearing capacity q_{max} and the end bearing capacity factor N_c ($=q_{max}/\sigma_c$)- The ratio of the shaft base displacement s_b at q_{max} to the shaft diameter B is also included in Table 3.16. A number of issues that need be considered when studying the relationship between the end bearing capacity and the unconfined compressive strength of intact rock are as follows:

1. Different interpretations of the load test data will give different capacities. For the test shafts in Table 3.16, different interpretation methods were used. For example, Goeke and Hustad (1979) took the load at plunging failure as the ultimate capacity orthe shaft (plunging failure is defined as the point at which additional load cannot be applied to the shaft without experiencing continuous movement), while Jubenville and Hep worth (1981) defined the ultimate capacity of the shaft as the load at which the shaft head displacement reached 10% of the shaft diameter. Therefore, some uncertainties and variabilities are likely to be included in the database. However, the general trend reflected by the database will be useful.

2. The unconfined compressive strength is a property of the intact rock, not of the rock mass. Clearly rock mass discontinuities must affect the end bearing capacity. Unfortunately, relevant information on (his factor is unavailable for most of the cases in Table 3.16.

3. The conditions below the base of the shaft also influence the end bearing capacity. If the base of the drilled hole cannot be cleaned, little or no end bearing support will be developed. For all the test shafts in Table 3.16, the base of the drilled hole was cleaned.

4. Different methods are used to separate the side shear resistance from the end bearing capacity in load tests.

5. Clearly it would be interesting (o have a relatively narrowly defined shaft base displacement which one can associate with the end bearing capacity. However, the values of s_b/B in Table 3.16 indicate that the base displacement at q_{max}, ranges from 0.6 to 20% of the shaft diameter, i.e., 6 to 210 mm. It is thus difficult to say al this point what typical base displacements at q_{max} are. [For comparison, the displacement at ultimate side shear resistance is smaller; examination of more than 50 load-displacement curves for large-diameter drilled shafts showed that an average displacement of only 5 mm was necessary to reach initial failure of side shear resistance (Horvath et al., 1983)].

Table 3.15. Summary of database of shaft load tests (Zhang and Einstein, 1998a)

No.	Rock description	Diameter B (mm)	Depth to base L (m)	σ_c (MPa)	q_{max} (MPa)	$N_c = q_{max}/\sigma_c$	s_b/B[a] (%)	Reference
1	Mudstone, weak, clayey cretaceous	670	6	1.09	6.88	6.31	7.0	Wilson (1976)
2	Clayshale, with occational thin limestone seams	762	8.8	0.81	4.69	5.79	6.2	Goeke and Hustad (1979)
3	Shale, thinly bedded with thin sandstone layers	457	13.7	3.82	10.8	2.83	>10.0	Hummert and Cooling (1988)
4	Shale, unweathered	305	2.4	1.08	3.66	3.39	10.0	Jubenville and Hepworth (1981)
5	Gypsum[b]	1064	4.20	2.1	6.51	3.1	15-20	Leung and Ko (1993)
6	Gypsum[b]	1064	4.20	4.2	10.9	2.6	15-20	Leung and Ko (1993)
7	Gypsum[b]	1064	4.20	5.4	15.7	2.9	15-20	Leung and Ko (1993)
8	Gypsum[b]	1064	4.20	6.7	16.1	2.4	15-20	Leung and Ko (1993)
9	Gypsum[b]	1064	4.20	8.5	23	2.7	15-20	Leung and Ko (1993)
10	Gypsum[b]	1064	4.20	11.3	27.7	2.5	15-20	Leung and Ko (1993)
11	Till[c]	762	**	0.7	4	5.71	~1.3	Orpwood et al. (1989)
12	Till[c]	762	**	0.81	4.15	5.12	~4.6	Orpwood et al. (1989)
13	Till[c]	762	**	1	5.5	5.5	~1.4	Orpwood et al. (1989)
14	Diabase, highly weathered	615	12.2	0.52	2.65	5.1	>4.0	Webb (1976)
15	Hardpan (hard bearing till)[c]	1281	18.3	1.38	5.84	4.23	~4.0	Baker (1985)
16	Till[c]	1920	20.7	0.57	2.29	4.04	~1.9	Baker (1985)
17	Hardpan (hard bearing till)[c]	762	18.3	1.11	4.79	4.33	~7.3	Baker (1985)
18	Sandstone, horizontally bedded, shaley, RQD = 74%	610	15.6	8.36	10.1	1.21	>1.7	Glos and Briggs (1983)
19	Sandstone, horizontally bedded, shaley, with some coal stringers, RQD = 88%	610	16.9	9.26	13.1	1.41	>1.7	Glos and Briggs (1983)
20	Mudstone, highly weathered	300	2.01	0.65	6.4	9.8	6.4	Williams (1980)
21	Mudstone, highly weathered	300	1	0.67	7	10.5	5.7	Williams (1980)
22	Mudstone, moderately weathered	1000	15.5	2.68	5.9	2.2	1.1	Williams (1980)
23	Mudstone, moderately weathered	1000	15.5	2.45	6.6	2.7	0.7	Williams (1980)
24	Mudstone, moderately weathered	1000	15.5	2.45	7	2.9	0.6	Williams (1980)
25	Mudstone, moderately weathered	1000	15.5	2.68	6.7	2.5	0.7	Williams (1980)
26	Mudstone, moderately weathered	600	1.8	1.93	9.2	4.8	14.1	Williams (1980)
27	Mudstone, moderately weathered	1000	3	1.4	7.1	5	10.9	Williams (1980)
28	Shale	**	**	34	28	0.82	**	Thorne (1980)[d]
29	Sandstone	**	**	12.5	14	1.12	**	Thorne (1980)[d]
30	Sandstone, fresh, defect free	**	**	27.5	50	1.82	**	Thorne (1980)[d]
31	Shale, occational recemented moisture fractures and thin mud seams, intact core lengths 75 to 250 mm	**	**	55	27.8	0.51	**	Thorne (1980)[d]
32	Clayshale	740	7.24	1.42	5.68	4	~8.8	Aurora and Reese (1977)
33	Clayshale	790	7.29	1.42	5.11	3.6	~8.9	Aurora and Reese (1977)
34	Clayshale	750	7.31	1.42	6.11	4.3	~6.0	Aurora and Reese (1977)
35	Clayshale	890	7.63	0.62	2.64	4.25	~6.6	Aurora and Reese (1977)
36	Siltstone, medium hard, fragmented	705	7.3	9	13.1	1.46	~12.0	Radhakrishnan and Leung (1989)
37	Marl, intact, RQD = 100%	1200	18.5	0.9	5.3	5.89	**	Carrubba (1997)
38	Diabase Breccia, highly fractured, RQD = 10%	1200	19	15.0	8.9	0.59	**	Carrubba (1997)
39	Limestone, intact, RQD = 100%	1200	13.5	2.5	8.9	3.56	**	Carrubba (1997)

[a] s_b is the shaft base displacement at q_{max}.
[b] Gypsum mixed with cement is used as pseudo-rock in centrifuge tests. The diameters and depths are the equivalent prototype dimensions corresponding to 40 g in the centrifuge tests. The equivalent prototype depths to the shaft base range from 4.04 m to 4.35 m with an average of 4.20 m.
[c] Till is not a rock. It is used here because its σ_c is comparable to that of some soft rocks.
[d] These tests were not conducted by Thorne (1980). He only reported the data from other references

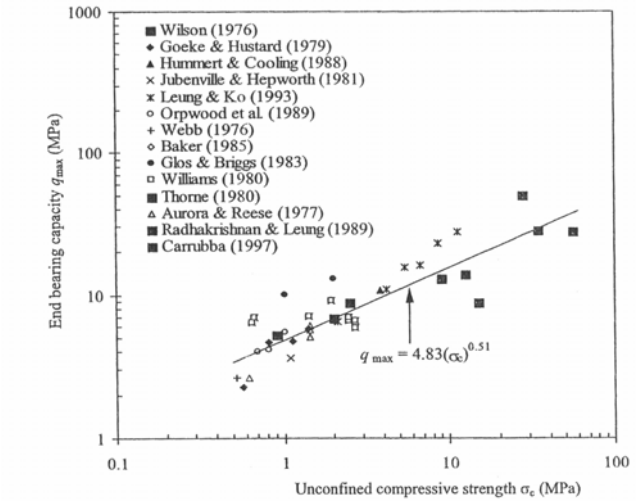

Figure 3.20. q_{max} versus σ_c (after Zhang and Einstein, 1998a)

All the load test data in Table 3.16 are plotted in Figure 3.20. A log-log plot is used. It can be seen that there is a strong relation between q_{max} and σ_c. Using linear regression, the relationship between q_{max} and σ_c is as follows: (The coefficient of determination, r^2=0.81)

$$q_{max} = 4.83(\sigma_c)^{0.51} \tag{3.25}$$

The coefficient of determination, r^2, is 0.81.

3.3. Summary

The design of axially loaded foundation piles in rock covers computation of ultimate load capacity and prediction of settlement under working load. Axially loaded drilled piles in rock are designed to transfer the structural loads to rock through side shear, through end bearing or through the combination of side shear and end bearing. It is also important to determine the pile's vertical displacements under working loads. There are many empirical ways to compute pile axial load capacity. It is possible to choose from these empirical formulas and design foundation piles according to the soil investigation data we have for a specific project. Although there are many empirical methods which are summarized in this chapter, most of these method's uses coefficients and proper coefficient selection for a specific project is hard most of the time.

4. CASE STUDY – PILE TESTING PROCEDURE FOR VERTICAL CAPACITY

As discussed in Chapter 2, the Mashattan Blocks A4 and A5 are planned to be constructed with foundation piles and mat foundation. According to soil investigations and superstructure loads, pile quantity, pile placement below the mat foundation and singular pile capacity is identified. Due to the fact that these high rise buildings are very heavy and very sensitive to excessive and variant settlement, the foundation project i.e. socket length of piles in Trace Formation verification need was realized. It is planned to execute two pile loading tests to verify if the performance criteria of selected pile lengths is satisfactory or not.

Ø800 mm diameter piles were required to maintain deep foundations in accordance with design. Two numbers of Static Pile Loading Tests (one test in A4, one test in A5) were performed in order to determine change of skin friction through Trace and Belgrade formations with respect to depth. The factor of safety for design was chosen two for vertical loads, therefore the ultimate load of 2x 3000 kN = 6000 kN was chosen as design verification load. Safe working and design verification loads are summarized in table 4.1.

Table 4.1. Safe working and design verification loads

DVL	:	Design Verification Load (test load)	6,000 kN
SWL	:	Safe Working Load	3,000 kN

4.1. Plant and Equipment for Special Static Load Test

Major items of plant and equipment are detailed below:

1. Hydraulic jack(s) with valid calibration report(s)
2. Hydraulic pump(s)
3. Hydraulic pressure gage(s) with valid calibration report(s)

4. Reaction frames including primary (main) and secondary frames
5. Steel bearing plate(s) (test plates) of sufficient thickness to prevent it from bending under the loads involved (but not less than 50mm)
6. Strain Gauges, fitting equipment and readout unit

4.2. Strain Gauges

The determination of strains in reinforced concrete members is the critical parameter in the calculation of working stresses.

4.2.1. Stress and Strain

The strength of a material is generally expressed in terms of ultimate stress, determined by applying increasing load to a sample of material until failure occurs. When a structural member is loaded, it undergoes a dimensional change. The member shortens with compressive stress and lengthens with tensile stress. The amount of dimensional change is always strictly proportional to the applied load in the elastic range, of which the upper limit is called the yield point. Above the yield point, an increase of load produces a permanent deformation (plastic range). In the elastic range, a normal stress σ applied to a surface results in a proportional strain ε (Hooke's Law). The ratio:

$$E = \frac{\sigma}{\varepsilon} \tag{4.1}$$

is defined as the Young modulus E. E is a constant for each material within the elastic range, therefore the load F is:

$$F = E \times \varepsilon \times A \tag{4.2}$$

where A is the cross section area of the member under stress.

The dimension change as a result of applied load is related to the length of the body, as follows:

$$\varepsilon = \frac{\Delta L}{L} \tag{4.3}$$

where L is the original length and ΔL is the change due to the applied load.

Strain measurement is usually obtained by means of an instrument called a strain gauge, normally manufactured in one of two varieties vibrating wire and resistive type.

Vibrating wire strain gauges consist of a length of high tensile steel wire, tensioned between two end blocks welded or affixed to the surface of, or embedded within, the structure being studied. Deformation of the structure will cause the two end blocks to move relative to each other, thus altering the tension of the steel wire. The tension of the wire is determined remotely, using an electromagnet to excite the wire and then by measuring its' resonant frequency of oscillation.

Where a strain gauge element is mounted onto a body of known section, a tension a will cause a change in electric resistance:

$$\frac{\Delta R}{R} = f(\frac{\Delta L}{L}) = f(\varepsilon) \tag{4.4}$$

Thermal compensation has to be considered to avoid measurement errors (thermal effects influence the length variation).

4.2.2. Vibrating Wire Strain Gauges

These consist of a protective stainless steel tube with two anchoring end blocks. Within the tube is a tensioned steel wire firmly fixed to the end blocks. The wire is excited by an external electromagnet housed in a small enclosure filled with resin. The electromagnet is located at the mid point of the tube. When the wire vibrates, the frequency is:

$$f = \frac{1}{2l}\sqrt{\frac{\sigma}{\rho}} \tag{4.5}$$

where l is wire length, σ is wire stress and ρ is material density. And therefore:

$$\sigma = \frac{4l^2 \times \rho}{g} \times f^2 \times 10^{-3} \tag{4.6}$$

where g is the gravity acceleration. For a tension variation the frequency will change of:

$$\Delta\sigma = \frac{4l^2 \rho}{g}(f^2 - f_0^2) \times 10^{-3} \tag{4.7}$$

where the factor $\frac{4l^2\rho}{g}$ is a constant K.

In most of the gauges, the wire length *l* is not equal to the distance "L" between the anchorages and therefore it is called gauge factor G:

$$G = K\frac{l}{L} \tag{4.8}$$

VK4000 type strain gauge is for surface application with anchor blocks which may be welded or glued, to rebar or to the surface of a structure(Figure 4.1). This gauge is supplied in an untensioned state and wire tensioning is done during the installation of the gauge on the blocks (fig. 4.2).

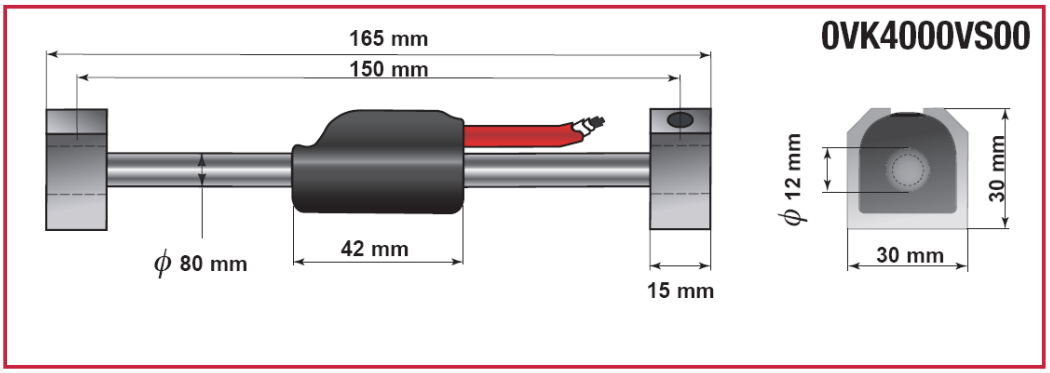

Figure 4.1. VK 4000 type strain gauge

Figure 4.2. Vibrating wire strain gauge for surface accessories

4.2.3. Installation Procedure

Vibrating wire strain gauges used for the tests were supplied fully sealed and tensioned with the plucking coil mounted.

(a) Vibrating Wire Strain Gauges Preliminary Checks

A preliminary check was done by connecting the gauge to the readout box (C6004VW SISGEO) and observing the displayed reading. The observed readings for the vibrating wire strain gauge embedment model should be around 1200 μsec (period mean) and around 830 Hz (frequency mean). The surface gauges needed to be tensioned using the proper jig, inserting the gauge in the jig so that the end cylinders are outside the jig. Once tensioned in the jig, stable readings were obtained from the readout. The reading without jig should be approximately 1130 μsec (period mean) and around 880 Hz (frequency mean), whereas with jig around 966 μsec (period mean) and around 1035 Hz (frequency mean). Pressure on the gauge ends should make the reading decrease when read in period units. Thermistor resistance was checked (the white and green lead wires) with an ohmmeter. Reading was checked against that which should be obtained at the existing ambient temperature.

(b) Installation of Surface Vibrating Wire Strain Gauge

A spacer bar was used to space two blocks to the correct distance (fig, 4.3). The vibrating wire strain gauge is attached to mounting blocks which have to be first arc welded to the surface in question (fig, 4.4).

Figure 4.3. Space bar to obtain correct distance between mounting blocks

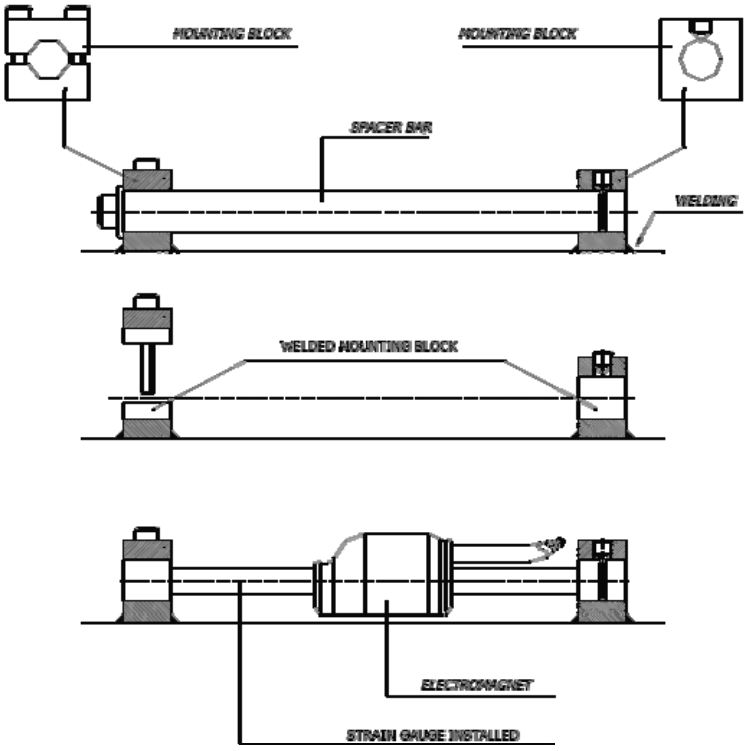

Figure 4.4. Installation scheme for vibrating wire strain gauge to a reinforcement

The installation procedure on piles is as follows:

a. The two mounting blocks are fitted over the ends of the spacer bar (Figure 4.4). Excessive tightening should be avoided as this may damage the spacer bar. A set of blocks is supplied: one is a simple block and the second is made of two pieces.

b. Clean the steel surface using wire brush to remove, rust, dirt, etc.

c. Using the spacer bar press the mounting blocks firmly against the steel surface. The edges of the blocks can now be welded. Avoid excessive heat and do not weld the flat end surface as this will prevent removal of the spacer bar. Where many gauges are being installed, it is advantageous to have more than one spacer bar.

d. After welding, cool the mounting blocks with a water soaked rag. Slacken the set screws and slide out the spacer bar.

e. Clean away all welding slag using a chipping hammer and wire brush.

f. If the gauges are to be protected by cover plates, then the studs should be welded in place before welding the mounting blocks (Figure 4.5).

Figure 4.5. Installation of vibrating wire strain gauge on piles

(c) Setting The Strain Gauge

Once the mounting blocks are welded in place, install the strain gauge as follows:

1. Unscrew the screws of the two piece mounting block and insert the gauge;
2. Insert the grooved end of the gauge in the other block;
3. Once the gauge is inserted in the blocks, tighten the set screw in the grooved end firmly and gently tighten the two screws on the other block;
4. Connect the instrument to the readout and switch on with the selector switch to position A.

The midpoint position is about 1200 μsec. If the gauge is to measure mainly compressive strains it should be pulled within a minimum reading of 750 μsec; if it is to measure mainly tensile strains it should be set within a maximum reading of 1500 μsec. Tension the gauge by pushing on the free end of the gauge. When the desired reading is obtained, the free end of the gauge is secured within the mounting block by tightening the two grub screws. The reading may alter slightly during this operation which is normal. Recheck that all grub screws are fully tightened. The gauge is supplied with the electric magnet permanently mounted in exactly in the right position. Corrosion of the weld points can be inhibited by applying a coat of rust preventative paint.

(d) Gauge Protection

The gauge may be protected from mechanical damage by a cover plate retained by studs or by welding. Studs or welds must be positioned a minimum of 15 cm from the gauge. Studs must not be over tightened otherwise surface distortion may occur, resulting in incorrect readings. In addition to that an additional protective shield was designed to protect the strain gauges from the tremie pipe(Figure 4.6).

Figure 4.6. Strain gauge protection reinforcement bars to avoid tremie pipe hits

(e) Cable Installation

The electric signal of each instrument is transmitted by means of an electrical cable. This cable is normally supplied in rolls(figure 4.7). Once the instrument has been installed, the cable must be installed correctly. This operation is as critical as the transducer installation. If the cable sheath is damaged by abrasion or cutting, loss of insulation will produce unstable readings.

Figure 4.7. Strain gauges with supplied specific length cables

(f) Junction Box Installation

Once the cable installation has been completed, it will then be possible to install junction boxes or terminal units(Figure 4.8). The boxes can be fixed in place using standard anchor bolts or on purpose made support brackets made on site according to requirements.

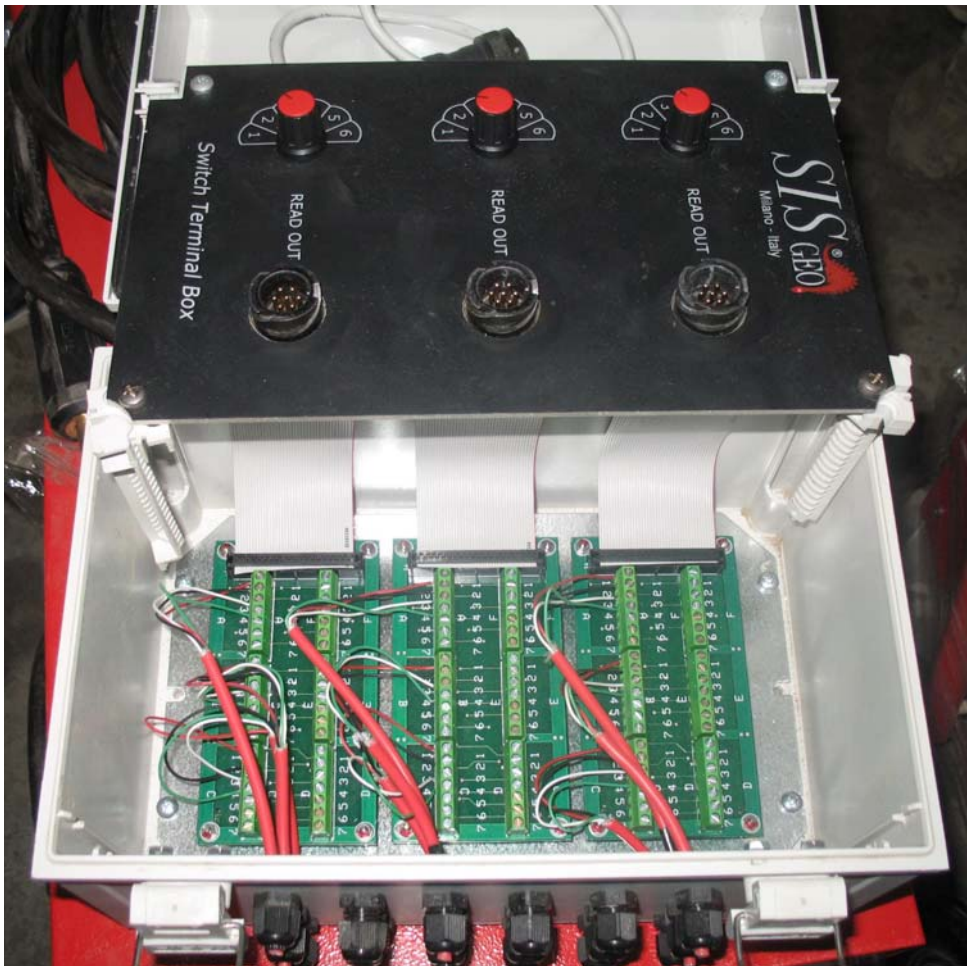

Figure 4.8. Cable connection between strain gauges and the junction box

(g) Taking Measurements

For strain gauges, the sensitivity factor is used to transform the electric output into engineering unit. Data acquisition systems record the data, which can be subsequently transferred to a computer for further processing and analysis. The manual read out C6004

VW, when connected to a vibrating wire strain gauge, displays either frequency, period, or direct measurement in με (figure 4.8).

Figure 4.9. C6004 VW manual read out

The measure taking procedure is as follows:

1. Connect the readout using the flying leads or with the connector if installed. The red and black clips are for the vibrating wire gauge, the white and green leads are for the thermistor (fig. 4.1);
2. Turn the display selector to the required position (see readout manual);
3. Turn the unit on and a reading will appear in the display window. The last digits may change by one or two units during reading. The reading shown on the display is updated every second;
4. The thermistor will be read and displayed in centigrade units when the display selector is rotated to the appropriate position.

(h) Initial Readings

All readings are referenced to an initial reading, so it is important that this initial reading is taken carefully. It is preferable to install gauges on steel members which are still in an unloaded condition, i.e., prior to their assembly into the structure. In this way, the initial readings correspond to zero load. Otherwise the initial readings will correspond to some unknown load level. The thermal coefficient of expansion of the steel of the vibrating wire is the same as for the steel of the structure to which the gauge is attached, so no temperature correction to the measured strain is required. However, this is only true if the

wire and the underlying steel structure are at the same temperature. If direct sunlight is allowed to impinge directly onto the gauge, then this could elevate the temperature of the wire above that of the surrounding steel and cause large changes in strain. It is always recommended to record the temperature every time the strain reading is made so that any strain effects, caused by temperature changes, can be evaluated. In order to facilitate the measurement of temperature, each vibrating wire strain gauge has a thermistor encapsulated along with the plucking coil.

(i) Welding Effects

Arc welding close to the gauges can cause very large strains on the steel structure. Thus, welding studs or reinforcement mesh on the steel cage near the instrument can cause large strain changes as can welding cover plates or protective channels, etc. over the gauges and cables. Always take gauge readings before and after any arc welding on the steel structure so that corrections can be applied to any apparent strain shifts.

(j) Data Processing

The C6004VW read out unit directly displays strain measurement in strain units when the rotary switch is in position D. This conversion is based on the following equation:

$$\mu\varepsilon = (f^2 \times 10^{-3}) \times G \tag{4.9}$$

where f is the resonant frequency of the wire and G is the gauge factor(it can be taken from the "compliance certificate")

The nominal value for vibrating wire strain gauges model VK4000VS is 3.3690. The change in strain $\Delta\varepsilon$ between the initial reading L0, and any subsequent reading Le, is obtained by calculating the difference between the two readings.

$$\Delta\mu\varepsilon = (L_e - L_0) \tag{4.10}$$

It should be noted that compressive strains are shown by decreasing readings (L_e-L_0<0), while tensile strains are shown by increasing readings (L_e-L_0>0).

Data processing requires the conversion from electrical to engineering units using a sensitivity factor given for each gauge on the calibration or control certificate. The sensitivity factor is calibration constant. The electrical value is divided by the sensitivity factor to obtain engineering units.

$$\mu\varepsilon = \frac{L}{S} \tag{4.11}$$

where:

$\mu\varepsilon = \frac{L}{S}$ = strain,

L = electrical reading,

S = sensitivity factor.

A reading taken at any time after installation is called “current reading” L_{es} while the “initial reading” or “zero reading” is indicated as L_0. Each reading has to be converted in a strain value, computed as follows:

$$\mu\varepsilon = \frac{(L - l_0)}{S} \tag{4.12}$$

where:

L = current reading

l_0 = reading taken before installation with instrument in air.

It is very important to take a very accurate l_0 values before installation because it is a good indicator that the instrument is working correctly. Moreover as l_0 has to be subtracted from all current readings it is advisable to take it very accurately several times to verify the repeatability of the instrument.

(k) Application of Resistive Strain Gauges for Pile Testing

The sample computing equations detailed as follows refer to the test scheme indicated in figure 5.1.

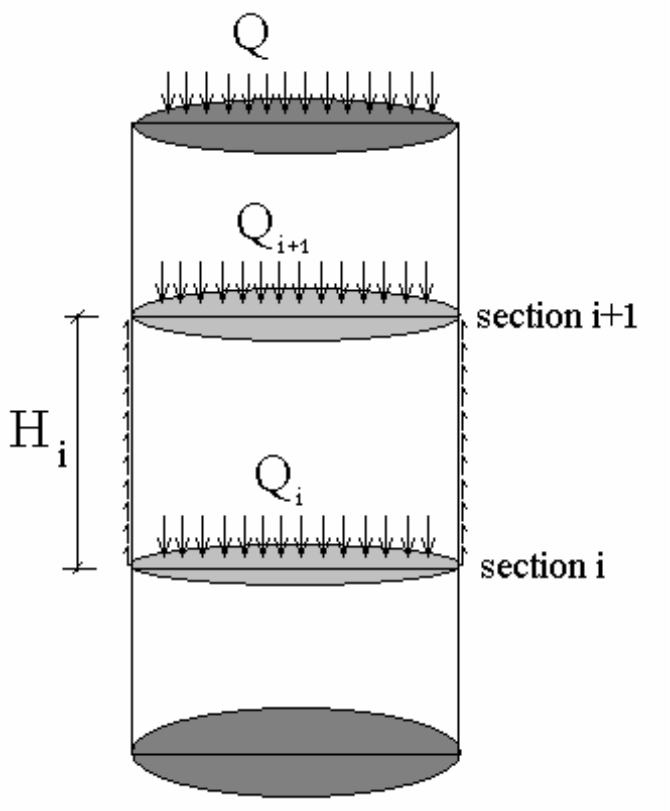

Figure 4.10. Data processing principle scheme

The imposed load Q is an incremental step of the applied load; it is assumed that the gauge readings are in engineering units($\mu\varepsilon$).

Axial stress in the i cross section can be calculated as:

$$\sigma_i = (Lmed_{es} - Lmed_0) \times 10^{-6} \times E_c \qquad (4.13)$$

where:

$Lmed_0$ = strain gauge average initial readings before load application

$Lmed_{es}$ = strain gauge average readings for a load Q

E_c = concrete Young's modulus

Axial load in i cross section can be calculated as:

$$Q_i = \sigma_i \times A \tag{4.14}$$

where A is the cross section area.

Average skin friction of the pile in the section between two instrumented cross sections can be calculated as:

$$\tau_i = \frac{(Q_{i+1} - Q_i)}{(\pi \times \phi \times H_i)} \tag{4.15}$$

where:

ϕ = pile diameter

H_i = length of the pile section

4.3. Pile Boring

The piles were bored using a hydraulic rotary rig. The stability of the excavation was maintained using steel casing as necessary. Necessary drilling tools were used to cleanly maintain specified min. 800 mm diameter. Prior to concreting the pile bases were cleaned using proper tools with rock teeth, to remove all detritus at the pile toe.

4.4. Placing Concrete

Concrete was transported from the mixer to the position of the pile in such a manner that segregation of the mix does not occur. The concrete was placed without such interruption as would allow previously placed batch to have achieved a stiffness which prevents proper amalgamation of the two concrete batches. Concrete was placed in the bored pile via a rigid delivery tube (tremie) to ensure that it falls vertically and centrally

down the shaft at the desired depth. The tremie was sufficiently long so that concrete leaving the lower end of the tremie fell no more than 2 m through the reinforcement cage.

4.5. Test Methodology

4.5.1. General

One number of tests with two loading and unloading loops was applied to an individual test pile. Test load (design verification load) was 6000 kN for both two tests. ASTM standard D 1143-81 was referenced during test. Hydraulic jacks acting against anchored reaction frame system was the apparatus for applying loads. Two number of reference beams for test pile and two number of reference beams for tension piles were used. For measuring movement, four pieces of dial gauges with 0.01mm precision were used. Three sets of strain gauges at three different elevations (-4.0m, -7.0m, -10.0m) are used to identify pile butt axial movements.

4.5.2. Test Pile

Each test pile was 11.20m in length and 800mm in diameter.

4.5.3. Reaction Piles

Maximum test load is obtained from four number of tension piles. Load applied to each pile at maximum load is 6000/4= 1500 kN. Each tension pile's length was 12.00m and each of them was 800mm in diameter.

4.5.4. Test Settlement

Static pile loading test placement is shown in Figure 4.11. Test pile was 800mm in diameter and bottom elevation of the pile was +55.90m. Working platform elevation for test pile boring was +68.58m.

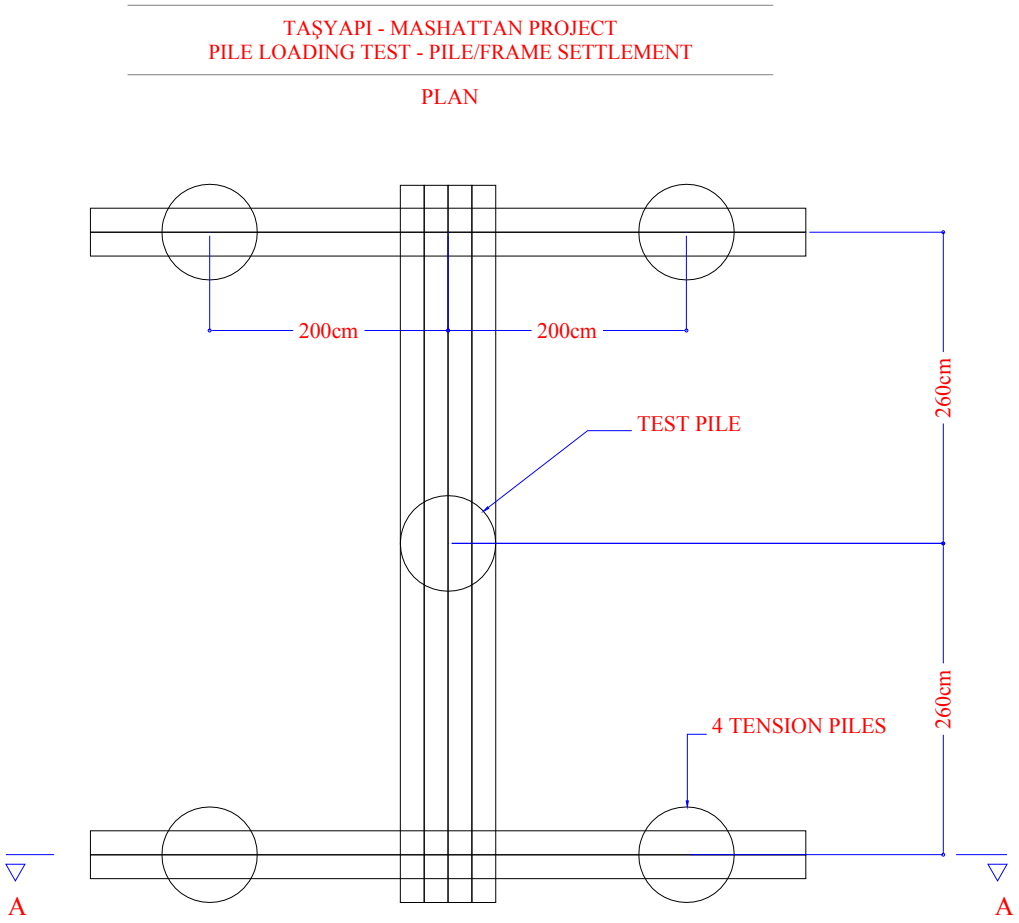

Figure 4.11. Pile loading test placement

Static pile loading test system section drawing is given in Figure 4.12. The test beams were attached to the tension piles with connections designed to adequately transfer the applied loads to the tension piles so as to prevent slippage, rupture or excessive elongation of the connections under maximum required test load.

Reaction system pictures are shown in Figure 4.12 and 4.13 respectively.

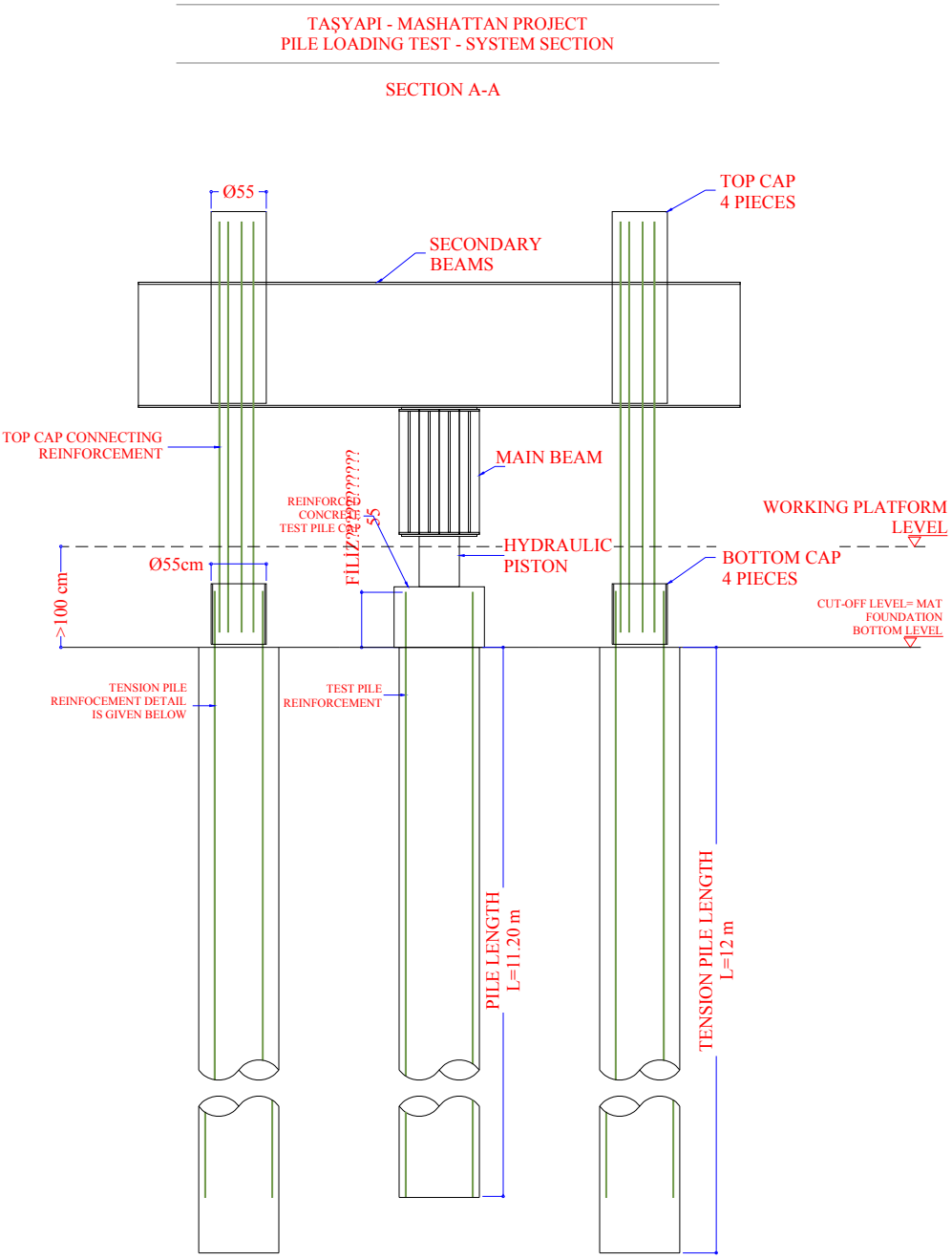

Figure 4.12. Pile loading test system section

Figure 4.13. Test pile reaction system site pictures

Loads were applied by two hydraulic jacks (Figure 4.14). Loads were applied to the central longitudinal axis of the reaction frame (beams and tension piles) to minimize the eccentric loading. Steel bearing plates, both at the tops of the jack rams (bottoms of the test beams) and bottoms of the jack rams (top of the reinforced concrete test pile cap). The total capacity of the tow hydraulic jacks were 2x4000= 8000 kN. The jack were placed on the test pile's reinforced concrete pile cap(Figure 4.16).

The complete jacking system including the hydraulic jacks, electrical powered hydraulic pump and pressure gauge was calibrated as a unit before tests. Both two

hydraulic jacks were of the same ram diameter, connected to a common manifold and pressure gauge and operated by a single hydraulic pump. As a multiple jacking system was used, each jack was fitted with a pressure gauge (in addition to the master pressure gauge) in order to detect malfunctions.

Figure 4.14. Hydraulic jacking system

Measure movements were achieved by using special apparatus. All reference beams were supported with supports firmly embedded in the ground at a clear distance not less than 2.50m from the test pile. Steel reference beams, which were sufficiently stiff, were chosen to support the instrumentation such that excessive variations in readings do not occur. One end of the each reference beam was let free to move horizontally as the beam length changes with temperature changes during the test. Dial gauges have 0-50mm travel with precision of 0.01mm. All dial gauges scales and reference points were clearly marked with reference number to assist in recording data accurately. All gauges attached to the test piles were mounted so as to prevent movement relative to the test pile caps during the test. Two parallel reference beams, one on each side of the test pile cap, was be oriented (figure 4.15).

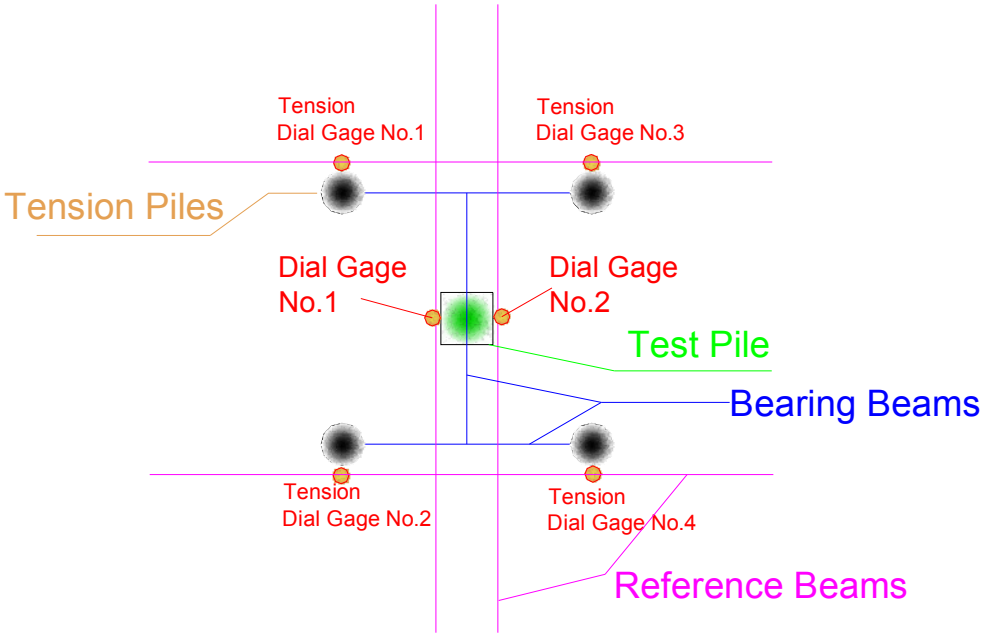

Figure 4.15. Reference beam placement for dial gage readings

Figure 4.16. Reinforced concrete pile cap with reinforcement extensions for deformation observations

5. CASE STUDY FOR PILE LOAD TESTS - EVALUATIONS FOR BLOCK A4

5.1. General

For Block A4, one number of tests with two loading and unloading loops was applied to an individual test pile on 15.05.2006. Test load (design verification load, (DVL) was 6000 kN for the test. ASTM standard D 1143-81 was referenced during test. Hydraulic jacks, with separate bar gauges, acting against anchored reaction frame system was the apparatus for applying load to the test pile. Two number reference beams for test pile and two number of reference beams for tension piles were used.

For measuring movement, four pieces of dial gauges with 0.01mm precision were used. Three sets (three straiun gauges per set) of strain gauges at three different elevations(-4.0m, -7.0m, -10.0m) are used to identify pile butt axial movements.

5.2. Loading Procedure

Loading was applied with two hydraulic Loading was applied with load steps 12.5% of design verification load. At each step 0, 5 minutes, 10 minutes, 15 minutes, 30 minutes dial gage readings and strain gauge measurements were taken(DENEY FOYU). For the fist loop, when safe working load (3000 kN) step was reached the deformations were observed for six hours and then unloading started. The load versus minimum waiting time chart is given in Table 5.1.

Table 5.1. Minimum waiting time for load steps

	Load (kN)	Minimum Waiting Time
First LoadingLoop	0.000 DVL (0 kN)	0 min
	0.125 DVL (750 kN)	30 min
	0.250 DVL (1500 kN)	30 min
	0.375 DVL (2250 kN)	30 min
	0.500 DVL (3000 kN)	360 min
	0.375 DVL (2250 kN)	15 min
	0.250 DVL (1500 kN)	15 min
	0.125 DVL (750 kN)	15 min
	0.000 DVL (0 kN)	120 min
Second Loading Loop	0.250 DVL (1500 kN)	30 min
	0.500 DVL (3000 kN)	30 min
	0.625 DVL (3750 kN)	30 min
	0.750 DVL (4500 kN)	30 min
	0.875 DVL (5250 kN)	30 min
	1.000 DVL (6000 kN)	720 min
	0.875 DVL (5250 kN)	15 min
	0.750 DVL (4500 kN)	15 min
	0.625 DVL (3750 kN)	15 min
	0.500 DVL (3000 kN)	15 min
	0.375 DVL (2250 kN)	15 min
	0.250 DVL (1500 kN)	15 min
	0.125 DVL (750 kN)	15 min
	0.000 DVL (0 kN)	240 min
	DVL: Design Verification Load	

With standard time intervals total loading-unloading time of the test was 28 hours 30 minutes. Several dial-gage readings were done through-out the test and displacement change due to time and due to load was obtained and plotted in figures 5.1, 5.2 and 5.3. The settlement values for critical phases are summarized in Table 5.2.

Table 5.2. Displacement values for critical loading phases

Test No:	**Maximum Displacement at 3000 kN (Safe Working Load) (mm)**	**Maximum Displacement at 6000 kN (Design Verification Load)** (mm)	**Permanent Settlement at 0 kN** (mm)
1	**1.08**	**6.01**	**2.40**

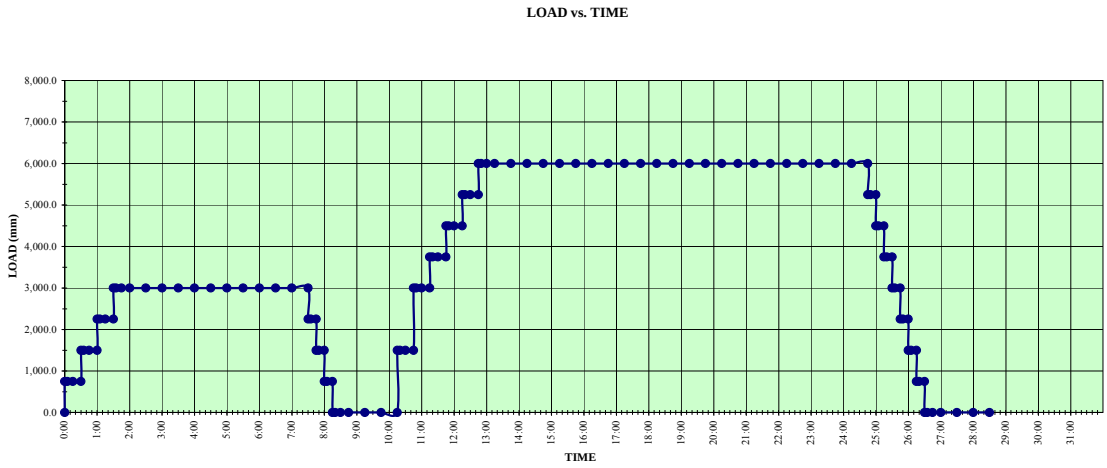

Figure 5.1. Change of applied load with respect to time

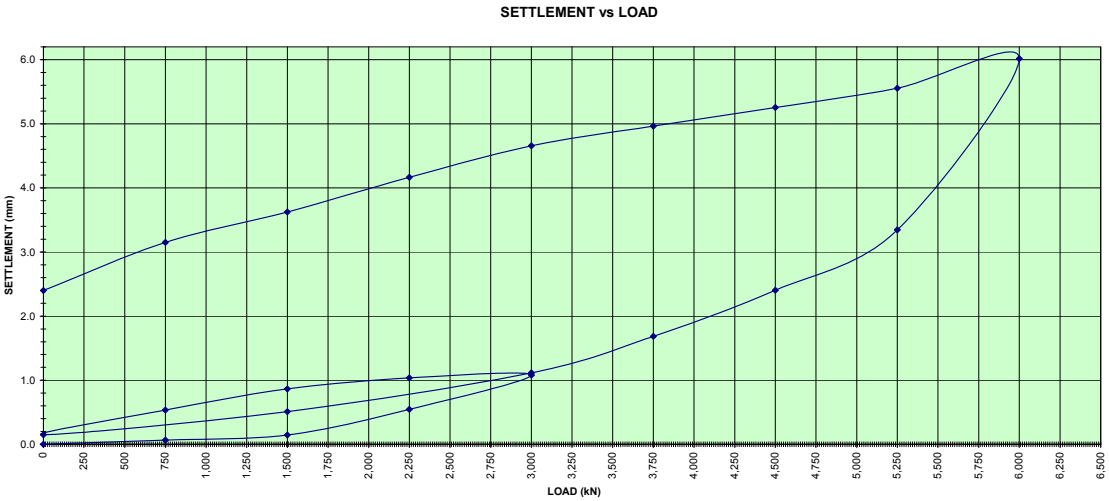

Figure 5.2. Change in displacement with respect to applied axial load

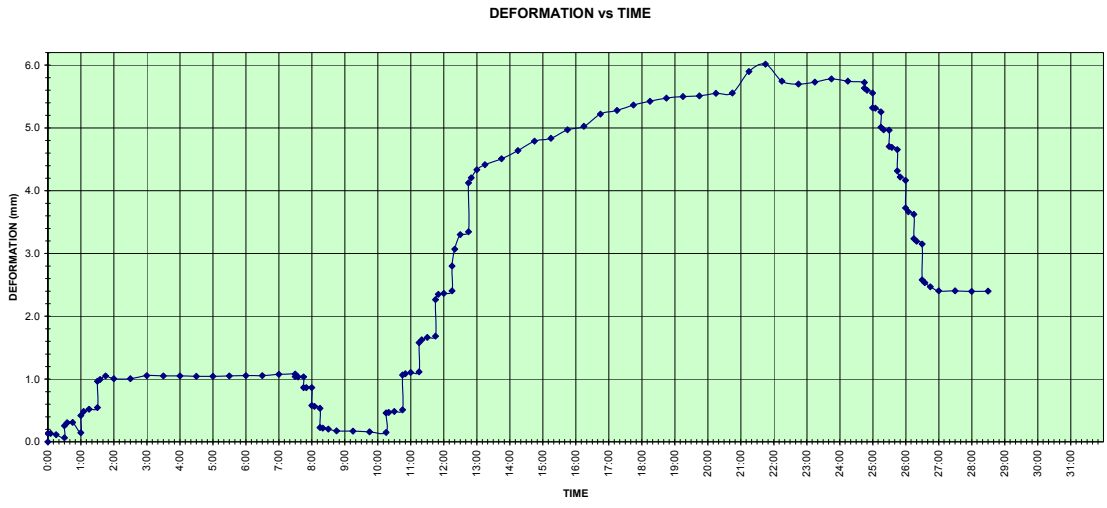

Figure 5.3. Change of deformation with respect to time

5.3. Skin Friction Measurements

Vibrating wire type strain gauge sets, three strain gauges per set, were placed on the pile reinforcement at -4.0m, -7.0m and -10.0m elevations in order to measure pile axial strain values. When the obtained frequency values, pile diameter and pile elastic modulus were processed, it was achieved to obtain pile axial stress with respect to depth. At the top of the pile, axial stress was more than the axial stress at deeper cross sections. This decrease in cross sectional axial stress means, the difference in stress between two strain gauge levels was carried out by skin friction between the control cross sections.

5.4. Evaluations

The cases where the average skin friction value of the pile was assumed linear with respect to depth and real obtained skin friction values are plotted together on the same graph in Figure 5.4. As shown in Figure 5.4 the measured skin friction values for the first 4m of the pile were less then the predicted average skin friction values and below 7m the measured skin friction values were greater than the expected values for the 3000 kN loading loop. Similarly for the 6000 kN loading loop the measured skin friction values for the first 4m of the pile were less then the predicted average skin friction values and below 7m the measured skin friction values were greater than the expected values. The measured skin friction values for the second loading loop(6000 kN) didn't exceed the measured skin friction values measured for the first loading loop(3000 kN).

Consequently it was observed that the for the first 4m of the pile, skin friction values were obtained less then the expected average skin friction values at both first and the second loading loops. Moreover the skin friction values below 7m depth were greater than the expected average skin friction values for both loading loops.

It is verified that for both 3000 kN and 6000 kN axial loads, all of the load was transferred to the soil body by skin friction and no end bearing was mobilized. The displacement was 1.08 mm under working load. Mobilization of skin friction resistance needs much less strain values and this was why the piles were projected to carry service

load by skin friction only to prevent excessive settlement for such a high and heavy structure.

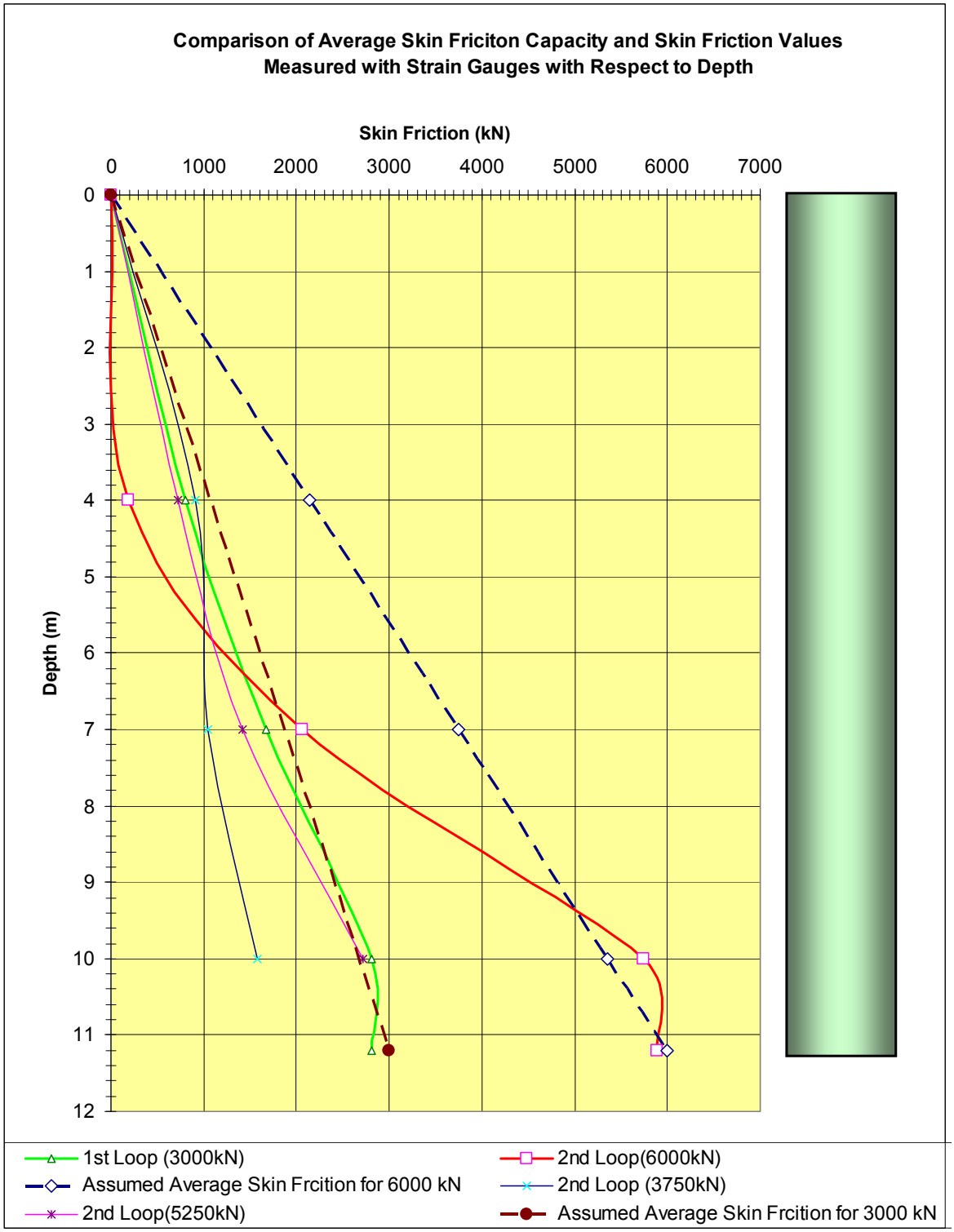

Figure 5.4. Comparison of average skin friction capacity and measured skin friction values (A4)

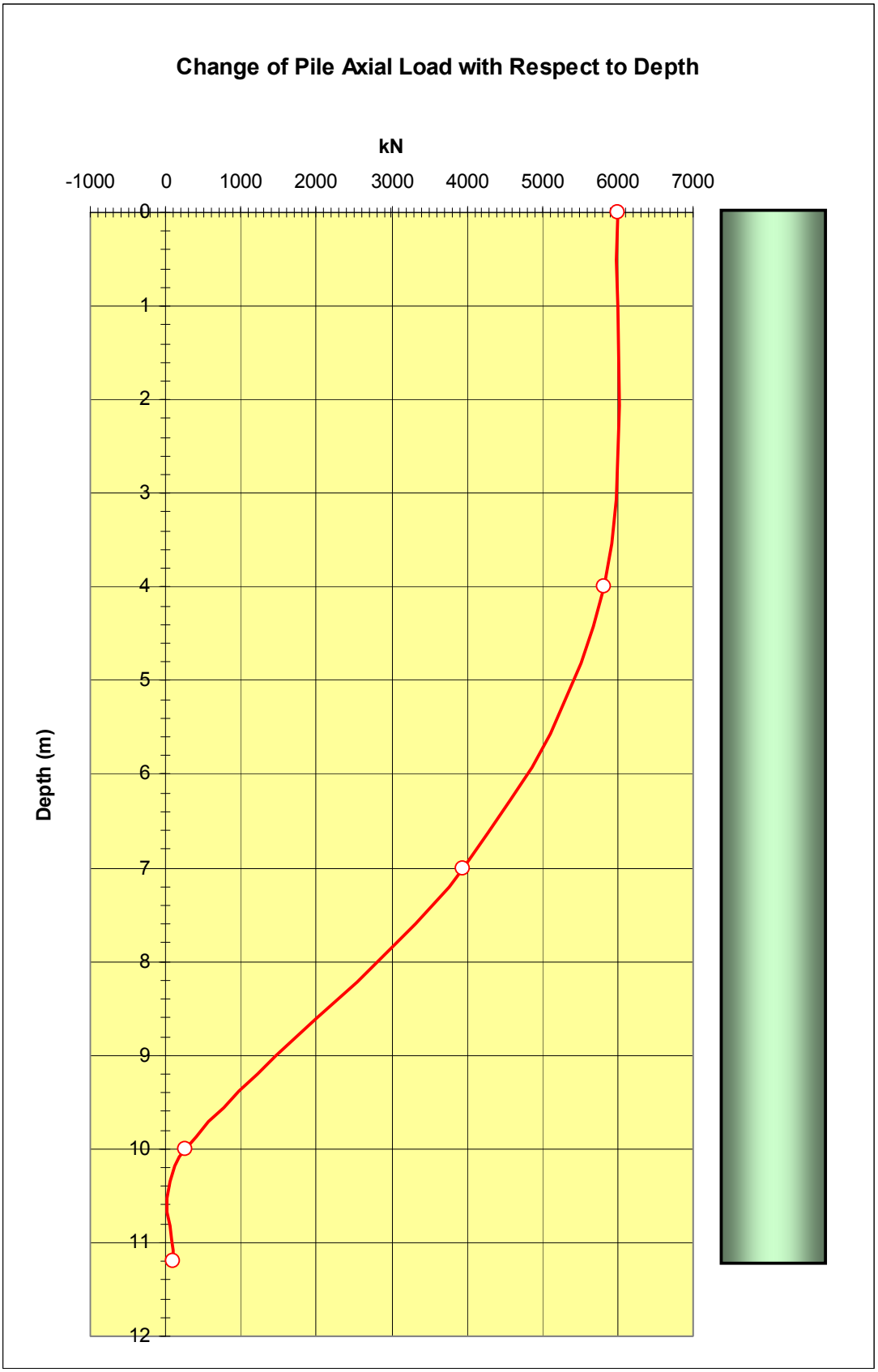

Figure 5.5. Change of the applied 6000 kN load on test pile with respect to depth (A4)

6. CASE STUDY FOR PILE LOAD TESTS - EVALUATIONS FOR BLOCK A5

6.1. General

For Block A5, one number of tests with two loading and unloading loops was applied to an individual test pile on 15.05.2006. Test load (design verification load, (DVL) was 6000 kN for the test. ASTM standard D 1143-81 was referenced during test. Hydraulic jacks, with separate bar gauges, acting against anchored reaction frame system was the apparatus for applying load to the test pile. Two number reference beams for test pile and two number of reference beams for tension piles were used.

For measuring movement, four pieces of dial gauges with 0.01mm precision were used. Three sets (three straiun gauges per set) of strain gauges at three different elevations(-4.0m, -7.0m, -10.0m) are used to identify pile butt axial movements.

6.2. Loading Procedure

Loading was applied with two hydraulic Loading was applied with load steps 12.5% of design verification load. At each step 0, 5 minutes, 10 minutes, 15 minutes, 30 minutes dial gage readings and strain gauge measurements were taken(DENEY FOYU). For the fist loop, when safe working load (3000 kN) step was reached the deformations were observed for six hours and then unloading started. The load versus minimum waiting time chart is given in Table 5.1.

With standard time intervals total loading-unloading time of the test was 28 hours 30 minutes. Several dial-gage readings were done through-out the test and displacement change due to time and due to load was obtained and plotted in figures ?.?, ?.? and ?.?. The settlement values for critical phases are summarized in Table 6.2.

Table 6.1. Displacement values for critical loading phases

Test No:	**Maximum Displacement at 3000 kN (Safe Working Load) (mm)**	**Maximum Displacement at 6000 kN (Design Verification Load)** (mm)	**Permanent Settlement at 0 kN** (mm)
1	**1.05**	**3.05**	**1.22**

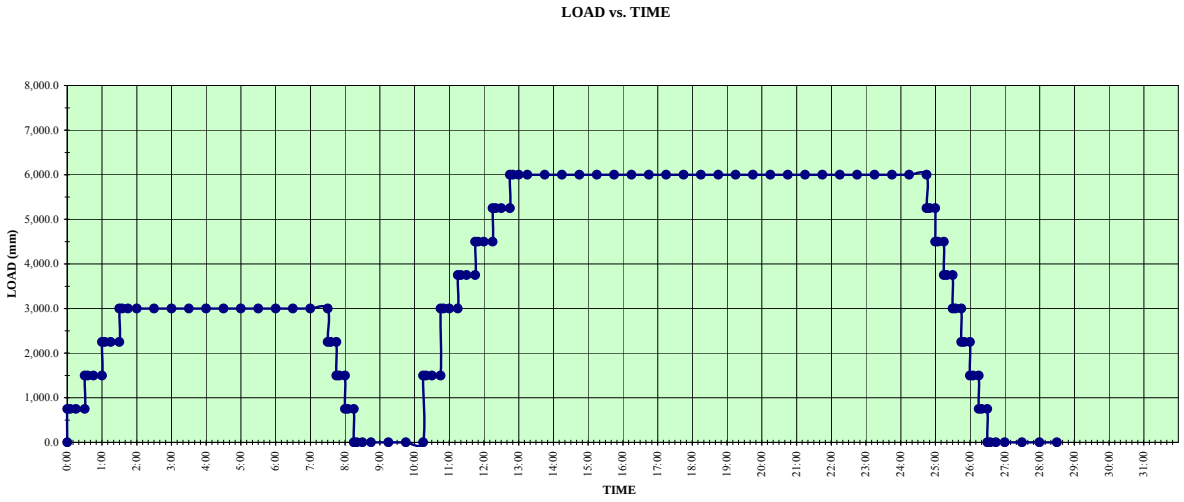

Figure 6.1. Change of applied load with respect to time

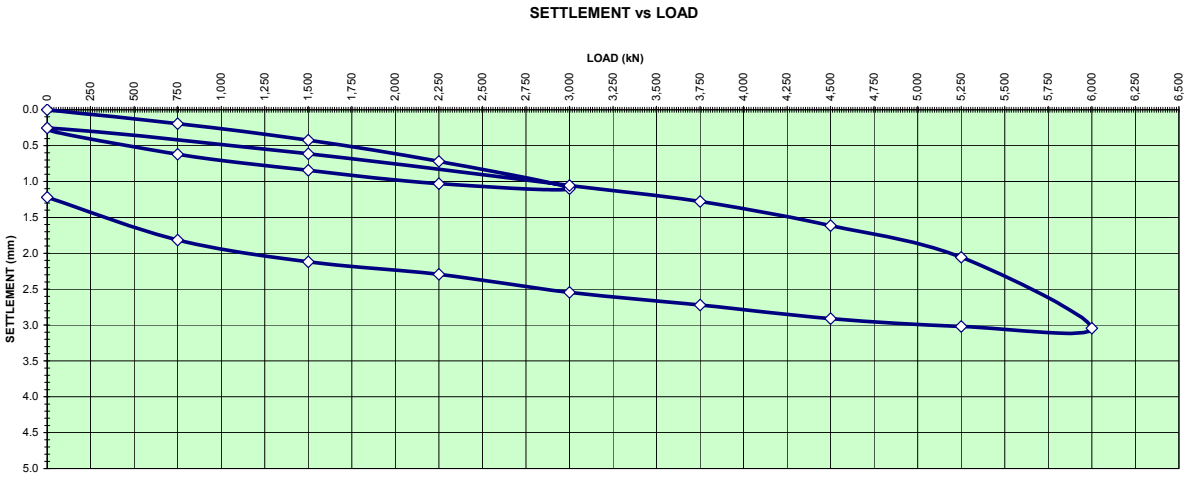

Figure 6.2. Change in displacement with respect to applied axial load

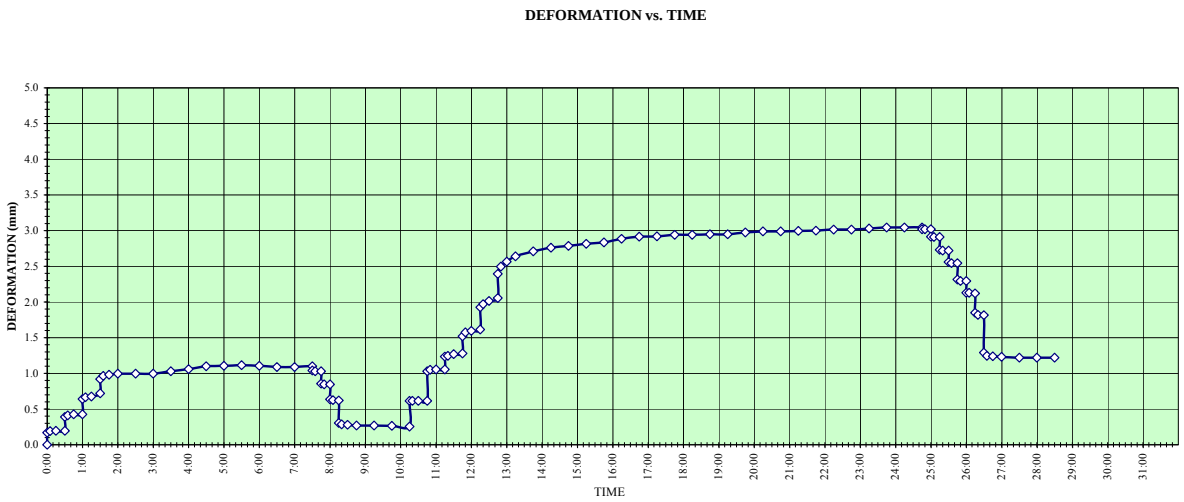

Figure 6.3. Change of deformation with respect to time

6.3. Skin Friction Measurements

Vibrating wire type strain gauge sets, three strain gauges per set, were placed on the pile reinforcement at -4.0m, -7.0m and -10.0m elevations in order to measure pile axial strain values. When the obtained frequency values, pile diameter and pile elastic modulus were processed, it was achieved to obtain pile axial stress with respect to depth. At the top of the pile, axial stress was more than the axial stress at deeper cross sections. This decrease in cross sectional axial stress means, the difference in stress between two strain gauge levels was carried out by skin friction between the control cross sections.

6.4. Evaluations

The cases where the average skin friction value of the pile was assumed linear with respect to depth and real obtained skin friction values are plotted together on the same graph in Figure 6.4. As shown in figure 6.4 the measured skin friction values for the first 4m of the pile were less then the predicted average skin friction values and below 7m the measured skin friction values were greater than the expected values for the 3000 kN loading loop. Similarly for the 6000 kN loading loop the measured skin friction values for the first 4m of the pile were less then the predicted average skin friction values and below 7m the measured skin friction values were greater than the expected values. The measured

skin friction values for the second loading loop(6000 kN) didn't exceed the measured skin friction values measured for the first loading loop(3000 kN).

Consequently it was observed that the for the first 4m of the pile, skin friction values were obtained less then the expected average skin friction values at both first and the second loading loops. Moreover the skin friction values below 7m depth were greater than the expected average skin friction values for both loading loops.

It is verified that for both 3000 kN and 6000 kN axial loads, all of the load was transferred to the soil body by skin friction and no end bearing was mobilized. The displacement of pile was 1.05 mm under design service load. Mobilization of skin friction resistance needs much less strain values and this was why the piles were projected to carry service load by skin friction only to prevent excessive settlement for such a high and heavy structure.

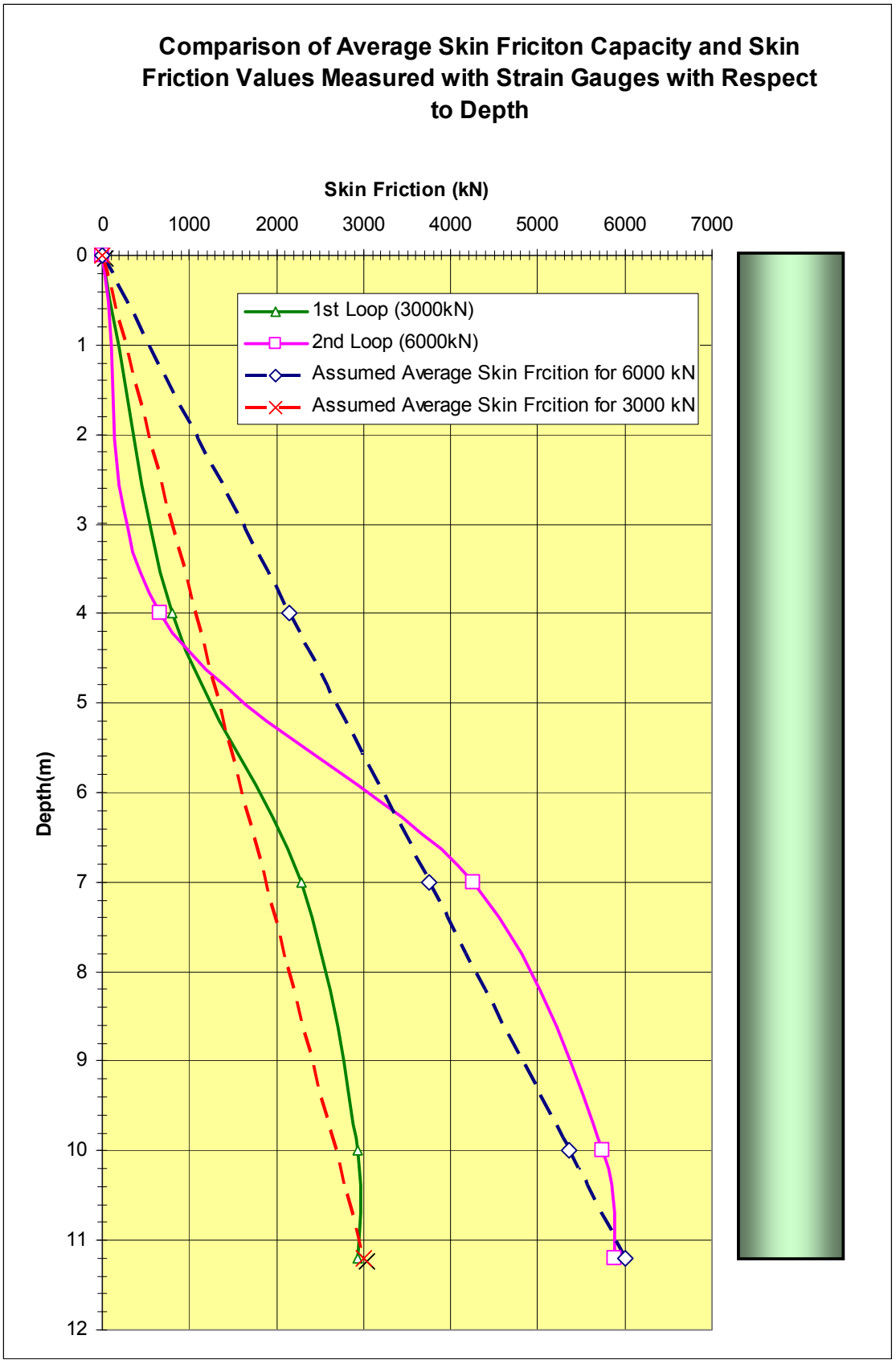

Figure 6.4. Comparison of average skin friction capacity and measured skin friction values (A5)

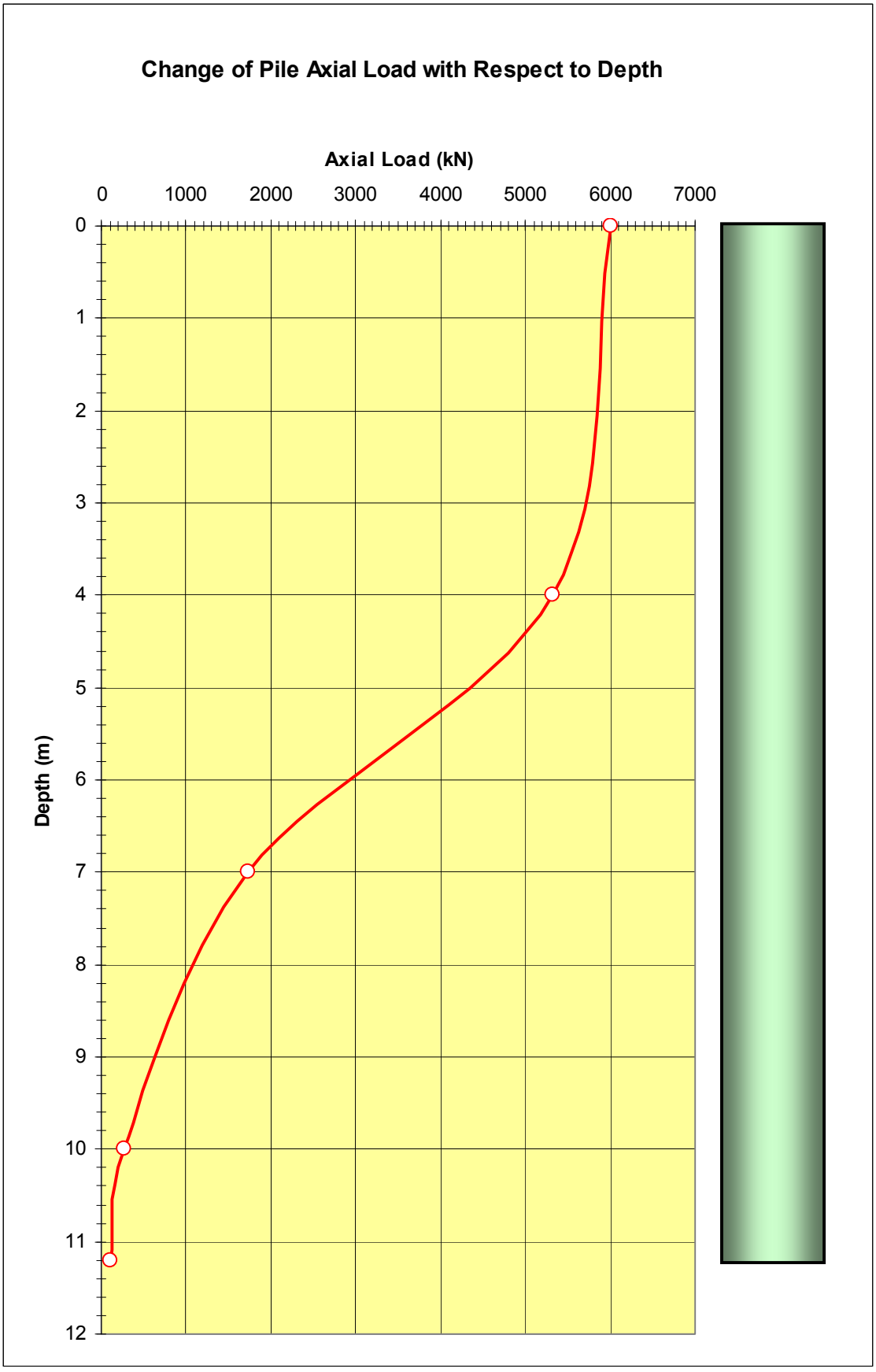

Figure 6.5. Change of the applied 6000 kN load on test pile with respect to depth (A5)

7. SUMMARY AND CONCLUSIONS

Drilled shafts are widely used to transfer heavy structural loads through the overburden soil to the underlying rock mass.

The primary difference between foundations in soil and those in rock is that rock masses contain discontinuities. Compared to intact rock, jointed rock masses have increased deformability and reduced strength. The existence of discontinuities in a rock mass creates anisotropy in its response to loading.

In cases where the rock mass can be identified very clearly, it is possible to use the empirical methods to design pile foundation system with appropriate performance criteria. If there are discontinuities in rock mass and a heavy superstructure is going to constructed design check plays a crucial role. Axially loaded drilled shafts in rock are designed to transfer structural loads to rock in one of the following ways: by side shear, by end bearing and combination of side shear and end bearing. When vertical displacement(especially variant displacement) is a major problem, pile is designed such that all load is transferred to rock mass by side shear(skin friction).

In this study piles in soft rock and behavior of piles in soft rock is studied and a case study is presented. In Maslak district of Istanbul, within Mashattan project, ten residential blocks with varying foundation levels are planned to be constructed. Formation at foundation level and strength of soil below foundation level for these ten blocks vary and cause a challenge in foundation design. For blocks A4 and A5, foundation piles are designed to transfer the structure loads through Belgrad formation and Weathered Trace formation to the underlying Trace Formation (soft rock) only by side shear. Subsoil modeling of the investigation site and a brief explanation of the subject formations is covered in second chapter of this study.

There are many empirical ways to compute pile axial load capacity. It is possible to choose from these empirical formulas and design foundation piles according to the soil investigation data we have for a specific project. Although there are many empirical methods which are summarized in third chapter, most of these

method's uses coefficients and proper coefficient selection for a specific project is hard to estimate most of the time.

As case study a special pile testing procedure for vertical load capacity is identified in chapter four. Safe working load, design verification load, equipment for test and test methodology are summarized.

In the first loading loop to the 3000 kN which was operated for A4 and A5 blocks test piles skin friction was mobilized in a specific proportion but very low amount of loading was transferred to the tip.

In the second loading loop of the A4 block test pile it is seen that the measured skin friction at the 6.2m depth is equal to the expected value. In the 2nd loading loop of the A5 block test pile it is seen that the measured skin friction at the 9.5m depth is equal to the expected value. Mobilized mean skin friction values (under 6000 kN loading test) for the Belgrade formation are very low, for the weathered Trace formation at A4 and A5 blocks are 35 kN/m^2 and 70 kN/m^2 respectively, on the other hand, for the Trace formation at A4 and A5 blocks are 700 kN/m^2 and 300 kN/m^2 respectively. The pile displacements under the design service loads in both tests were 1.08 mm and 1.05 mm which are within well below the acceptable limits for the high rise structures.

REFERENCES

CGS, 1985, *Canadian Foundation Engineering Manual.* Part 2 (2nd ed.) Canadian Geotechnical Society, Vancouver, Canada.

D1143-81 Standart Test Method for Piles Under Static Axial Compressive Load, 1994, American Society of Testing Materials (ASTM), West Conshohocken.

Kaya, O., 1973, "The Devonian and Lower Carboniferous Stratigraphy of The Istınye, Bostancı and Büyükada Subareas", Paleozoik of Istanbul, Bornava.

Kulhawy, F. H. and R. T. Goodman, 1980, Design of Foundation on Discontinous Rock. *Int. Conf. On Struc. Found. on Rock,* Ed: P.J.N. Pells, Balkema, Rotterdam, 209-220.

Ternk, Z., B. Akyürek, 1987, "Explanatary Text of The Geological Map of Turkey", MTA, Ankara, 1987.

Toğrol, E. and O. Tan, 2003, *Kazıklı Temeller,* Birsen Yayınevi, Istanbul.

Toh, C. T., T.A. Ooi, H.K. Chiu, S.K. Chee and W.N. Ting, 1989, Design parameters for bored piles in a weathered sedimentary formation. *Proc. 12th Int. Conf. On Soil Mech. And Found. on Rock, Sydney, 1, 223-233.*

Yılmaz, H. and T. Durgunoğlu, 2006, "Yumuşak Kayalarda Kazıkların Soketlenme Boyu-Bir Vaka Analizi", Zemin Mekaniği ve Temel Mühendisliği Onbirinci Ulusal Kongresi, Karadeniz Teknik Üniversitesi, Trabzon, 7-8 Eylül 2006.

Yıldırım, M. and E. Savaşkan, 2003, "A New Approach to The Stratigraphy of The Tertiary Sedimantary Formations in Istanbul and Their Engineering Properties", Geology Symposium of Istanbul, Istanbul.

ZETAS Zemin Teknolojisi A.S., 2005a, “Maslak Vadi Konutları, Ayazağa/Istanbul Pafta 2, Ada 1, Parsel 105 Zemin Etüdü ve Temel Mühendisliği Değerlendirme Raporu”,.01.04.2005.

ZETAS Zemin Teknolojisi A.S.,2005b, “Mashattan Projesi Ayazağa/Istanbul A4 Blok İlave Zemin Etüdü ve Temel Mühendisliği Değerlendirme Raporu”, 19.12.2005.

ZETAS Zemin Teknolojisi A.S.,2005c, “Mashattan Projesi Ayazağa/Istanbul A5 Blok İlave Zemin Etüdü ve Temel Mühendisliği Değerlendirme Raporu”, 14.12.2005.

ZETAS Zemin Teknolojisi A.S., 2006a, “Mashattan Projesi A4 Blok Kazık Yükleme Deneyi Dökümantasyon ve Değerlendirme Raporu”, 22.05.2006.

ZETAS Zemin Teknolojisi A.S., 2006b, “Mashattan Projesi A5 Blok Kazık Yükleme Deneyi Dökümantasyon ve Değerlendirme Raporu”, 09.03.2006.